

NEAR-INFRARED AND MÖSSBAUER STUDY OF
CATION SITE OCCUPANCIES IN TOURMALINES

by

Henry Francis Simon

S.B., United States Military Academy
(1966)

SUBMITTED IN PARTIAL FULFILLMENT OF THE
REQUIREMENTS FOR THE DEGREE OF
MASTER OF SCIENCE

at the

MASSACHUSETTS INSTITUTE OF TECHNOLOGY

May, 1973

Signature of Author _____
Department of Earth and Planetary Sciences, May 11, 1973

Certified by _____ Thesis Supervisor

Accepted by _____
Chairman, Departmental Committee on Graduate Students

Lindgren
WITHDRAWN
FROM
JUN 28 1973
MIT LIBRARIES

NEAR-INFRARED AND MÖSSBAUER STUDY OF
CATION SITE OCCUPANCIES IN TOURMALINES

BY

Henry Francis Simon

Submitted to the Department of Earth and Planetary Sciences
on May 11, 1973, in partial fulfillment of the requirements
for the Degree of Master of Science.

ABSTRACT

Mössbauer and near-infrared spectral measurements have been made on several tourmaline minerals representing both the elbaite-schorl and dravite-schorl series. The specimens were characterized by cell dimension measurements, and by partial chemical analyses by electron microprobe.

Mössbauer data for the iron-bearing specimens further substantiated the presence of ferrous and ferric cations in both the larger 9(b) and smaller 18(c) octahedral sites in the tourmaline structure. Quantitative estimates of site occupancies of the ferrous ions were based on relative areas under component doublets in the Mössbauer spectra, fitted with Lorentzian curves. Mössbauer spectroscopy also revealed that the oxidation process of ferrous iron in tourmalines is favored in the 18(c) site.

Optical/near-infrared spectroscopy indicated that the $\text{Fe}^{2+} \rightarrow \text{Fe}^{3+}$ intervalence transition band occurs at $\sim 15000 \text{ cm}^{-1}$ in tourmalines, and not at $\sim 14000 \text{ cm}^{-1}$ as previously suggested. Component Gaussian curves fitted to tourmaline spectral envelopes conformed with earlier assignments of the 9000 cm^{-1} band to a crystal-field transition within Fe^{2+} ions in the tourmaline 9(b) sites. Curve fitting also led to the resolution of an additional peak at 14000 cm^{-1} , which was attributed to a crystal-field transition within Fe^{2+} ions in the tourmaline 18(c) sites.

Correlations between the Mössbauer and the electronic spectral data confirmed the assignment of the 14000 cm^{-1} peak to

ferrous iron located in the tourmaline 18(c) octahedral site. Trends in the relative area ratios of assigned ferrous iron doublets in the Mössbauer spectra and of the designated ferrous iron spectral peaks in the near-infrared spectra were in satisfactory statistical agreement, leading to the conclusion that the two spectroscopic methods complement one another in the study of cation distributions in these iron-bearing silicate minerals.

The investigation of the first-overtone, O-H bond, stretch spectra engendered qualitative trends only. The spectra, though very complex, did display certain peak trends attributable to lithium (~1403 nm), magnesium (~1426 nm), ferrous iron (~1442 nm) and aluminum (~1470 nm).

This study, based on data from three independent spectral techniques, demonstrates the interchangeability of divalent and trivalent iron cations over the smaller 18(c) and larger 9(b) octahedral sites in the tourmaline structure, which might not be predicted from ionic radius criteria.

THESIS SUPERVISOR: Roger G. Burns

TITLE: Professor of Earth and Planetary Sciences

ACKNOWLEDGMENTS

The author thanks Professor C. Frondel for supplying the specimens from mineral collections at Harvard University. Thin sections were mounted and ground to specifications by H. Thompson, Harvard University. Valuable advice and assistance on the Cary 17 spectrophotometer was rendered by Rateb Abu-Eid. Professor J. Dickey advised and assisted the author in the electron microprobe analyses. Constructive comments and advice on Mössbauer data analysis was rendered by E. Whipple. A special thanks goes to Frank Huggins for his continued advice and assistance through the whole data collection period, and his valuable comments on the manuscript. To Mrs. Michelle Huggins and Mrs. Judith Simon, a sincere vote of gratitude is rendered by the author for the final preparation of the text and figures, respectively.

And in saving the most heartfelt thanks to last, I wish to express my sincere gratitude and appreciation to Professor R.G. Burns, whose genuine interest and infinite patience were only surpassed by his professional knowledge and invaluable criticism in directing and encouraging the author throughout the totality of this investigation.

DEDICATION

I respectfully dedicate this thesis to my wife, Judith Ann, with the sincere anticipation that this significant venture in time and effort will be just the first of many such endeavors that we will eagerly await and conquer together as we live our lives as one before God and man.

TABLE OF CONTENTS

<u>Chapter No.</u>		<u>Page No.</u>
1	Introduction	7
2	Crystal Structure	11
3	Experimental	17
	3.1 Cell Dimensions	17
	3.2 Chemical Analysis	17
	3.3 Mossbauer Spectroscopy	21
	3.4 Optical/Near-infrared Spectroscopy	22
	3.5 First-overtone, O-H Bond, Stretch Spectra	23
4	Results	46
	4.1 Mossbauer Spectroscopy	46
	4.2 Optical/Near-infrared Spectroscopy	50
	4.3 First-overtone, O-H Bond, Stretch Spectra	53
5	Discussion	59
	5.1 Mossbauer Spectroscopy	59
	5.2 Optical/Near-infrared Spectroscopy	60
	5.3 Comparison of Mossbauer - Optical/ Near-infrared Results	60
	5.4 First-overtone, O-H Bond, Stretch Spectra	62
	<u>References</u>	64

Chapter 1

INTRODUCTION

The tourmaline group of minerals is an example of common, hard, chemically resistant and complex, iron-bearing borosilicates. It may be represented by the idealized formula $XY_3Z_6B_3Si_6O_{27}(OH,F)_4$, of which there are three such formula units per unit cell. The tourmaline structure belongs to the space group R3m. The X site is in 10-fold co-ordination with point symmetry 3m, labeled 3(a). The Y and Z sites are in 6-fold co-ordination with point symmetry m, labeled 9(b), for the larger Y site, and with point symmetry 1, labeled 18(c) for the smaller Z site. (Wyckoff's notation in the International Tables for X-Ray Crystallography, 2nd ed., vol. I, p. 266.) The X cations are Na^+ , Ca^{2+} , and K^+ ; the Y cations may be Li^{1+} , Mg^{2+} , Fe^{2+} , Mn^{2+} , Fe^{3+} , Al^{3+} , Ti^{3+} , and Ti^{4+} ; while the Z cations have been largely assumed to be Al^{3+} , except in some Al deficient tourmalines in which Mg^{2+} and Fe^{3+} were assumed to fill the Z site (Buerger, Burnham and Peacor, 1962; Frondel, Biedl and Ito, 1966). Recently, crystal structure determinations of the ferric tourmaline buergerite, $NaFe_3^3+Al_6B_3Si_6O_{31}$, by X-ray (Barton, 1969) and neutron (Tippe and Hamilton, 1970) diffraction, and by magnetic susceptibility (Tsang, Thorpe, Donnay and Senftle, 1971), demonstrated that Fe^{3+} atoms are located in both the Y and Z sites in the tourmaline structure.

With the advent of positive identification of iron in two differing sites in the crystal structure, tourmalines became a prime candidate for study using Mössbauer spectroscopy.

A fairly recent addition to the tools of the Earth Scientist, Mössbauer spectroscopy has become an important means of analyzing and interpreting the crystal chemistry of iron in minerals (Burns, 1968; Bancroft and Burns, 1969; Burns and Greaves, 1971; Vaughan and Burns, 1972). The background for its discovery and the principles of the effect have been discussed in great detail in published literature (Frauenfelder, 1962; Wertheim, 1964; Fluck, 1964; Duncan, 1965). Though the full potentials of the effect have most likely not yet been discovered, two important applications to mineralogical problems have been successfully employed. First, Mössbauer spectroscopy provides a rapid method for characterizing the oxidation state and co-ordination number of iron atoms in minerals. Second, Mössbauer experiments may be used to detect cation ordering and to estimate site populations in complex crystal structures (Bancroft and Burns, 1967; Bancroft, Burns and Maddock, 1967; Bancroft, Burns, Maddock and Strens, 1966; Bancroft, Burns and Howie, 1967).

Tourmalines also contain transition metal ions, such as Ti^{4+} , Cr^{3+} , Mn^{3+} , Fe^{2+} , and Fe^{3+} , and are therefore susceptible to crystal field spectra (Burns, 1970). The absorption spectra of pink (Wilkins, Farrell and Naiman, 1969; Manning, 1969),

blue (Faye, Manning and Nickel, 1968; Wilkins et al., 1969), green (Faye et al., 1968; Wilkins et al., 1969), brown (Wilkins et al., 1969; Manning, 1969), and black (Manning, 1969) tourmalines have been recorded. The pink, blue, and green tourmalines fall on the elbaite-schorl $\text{Na}(\text{Li}, \text{Al}, \text{Fe})_3\text{Al}_6\text{B}_3\text{Si}_6\text{O}_{27}(\text{OH}, \text{F})_4$ join, while the brown and black specimens are usually located on the dravite-schorl $\text{Na}(\text{Mg}, \text{Fe})_3\text{Al}_6\text{B}_3\text{Si}_6\text{O}_{27}(\text{OH}, \text{F})_4$ segment.

Considerable debate has arisen concerning the interpretation of the two prominent iron absorption bands located in the 9000-14000 cm^{-1} region of the electro-magnetic wave spectrum. Based on dravite metal-oxygen distances in the refined crystal structure (Buerger et al., 1962), and the calculated value of the crystal field splitting parameter Δ , the bands were assigned to the ${}^5\text{T}_{2g} \rightarrow {}^5\text{E}_g$ transition of Fe^{2+} in the 9(b) site with a tetragonal splitting of the ${}^5\text{E}_g$ orbitals of approximately 5000 cm^{-1} (Wilkins et al., 1969). An alternate assignment has been made for the 14000 cm^{-1} band to an $\text{Fe}^{2+} \rightarrow \text{Fe}^{3+}$ intervalence transition between neighboring Fe^{2+} ions in 9(b) sites and Fe^{3+} ions in 18(c) sites in the structure, due to overlapping T_{2g} orbital lobes in the (001) plane (Faye et al., 1968; Robbins and Strens, 1968; Manning, 1969). And still a third alternative has been proposed for the 14000 cm^{-1} band, in that it is the result of the Jahn-Teller effect in the E_g orbitals, dealing with orbital energy transitions (Wilkins et al., 1969). A recent study of buergerite (Manning, 1969) also indicated that the relative intensities of the 14000 and 9000 cm^{-1} bands were

virtually unaffected by the amount of Fe^{3+} in the structure, in comparing it with green and blue tourmaline spectra. These results, though differing in interpretation, imply that there are Fe^{2+} and Fe^{3+} ions in detectable amounts for Mössbauer spectroscopy application.

The first part of this study will concern itself with the problem of the assignment of the 14000 cm^{-1} band from correlations with data obtained from Mössbauer and optical/near-infrared spectroscopy.

Tourmalines also contain hydroxyl ions, located in the O_1 and O_3 (Buerger et al., 1962) sites, which are apices of the 9(b) and 18(c) site octahedra. Previous work on amphiboles has indicated that site occupancies can be deduced from vibrational spectra of O-H bond, stretch bands in the infrared regions of the electro-magnetic wave spectrum (Burns and Strens, 1966; Bancroft and Burns, 1969; Burns and Greaves, 1971). Recent work has physically described and given bond assignments to the fundamental bands in the $3900\text{-}3500\text{ cm}^{-1}$ region (Plyusnina, Granadchikova and Voskresenskaya, 1969). The spectra of Wilkins et al. (1969) indicate differences in the first overtone bands in the 7100 cm^{-1} region, suggesting that cation site occupancy might be determined from a study of these first overtone bands. The second part of this study attempts to assign cation residency to, and to describe site occupancy for, the first overtone, O-H bond, stretch bands in tourmaline spectra.

Chapter 2

CRYSTAL STRUCTURE

The tourmaline structure belongs to the space group R3m. The structure consists of hexagonal rings of linked SiO₄ tetrahedra, with the tetrahedra pointing in the same direction, parallel to the c-axis (see Figure 1). The X site cations occupy the 3(a) position on the threefold axis at the center of the six-membered ring. The upper sheet consists of three components: (1) The Y site cations occupying the 9(b) position forming a cluster of three inner octahedra, each containing four oxygen and two (OH,F) ions, sharing edges to form a trigonal fragment of a brucite-like layer (Six oxygen atoms of this sheet are also the upper apices of the hexagonal ring of the SiO₄ tetrahedra.); (2) The Z site cations occupying the 18(c) position forming a cluster of six outer octahedra, each containing five oxygen and one (OH,F) ions, surrounding, and sharing edges with, the three inner octahedra; and (3) B-atoms in the 9(b) positions, forming BO₃ triangles which connect corners of two Z octahedra and a common corner of two inner Y octahedra (see Figure 2). The six outer Z octahedra form spiral chains along the c-axis by sharing edges with two similar octahedra, related by the 3₁ screw axis (Tsang and Ghose, 1973).

The 9(b) and 18(c) positions are displaced by 1-2 per cent

of the c parameter above the (001) projection plane. The 9(b) sites have two 9(b) and two 18(c) sites as nearest neighbors, while the 18(c) sites have one 9(b) and two 18(c) sites (see Figure 3).

The O_1 (OH_I) site is co-ordinated with three 9(b) and one 3(a) sites (see Figure 4a). The O_3 (OH_{II}) site is co-ordinated with one 9(b) and two 18(c) sites (see Figure 4b).

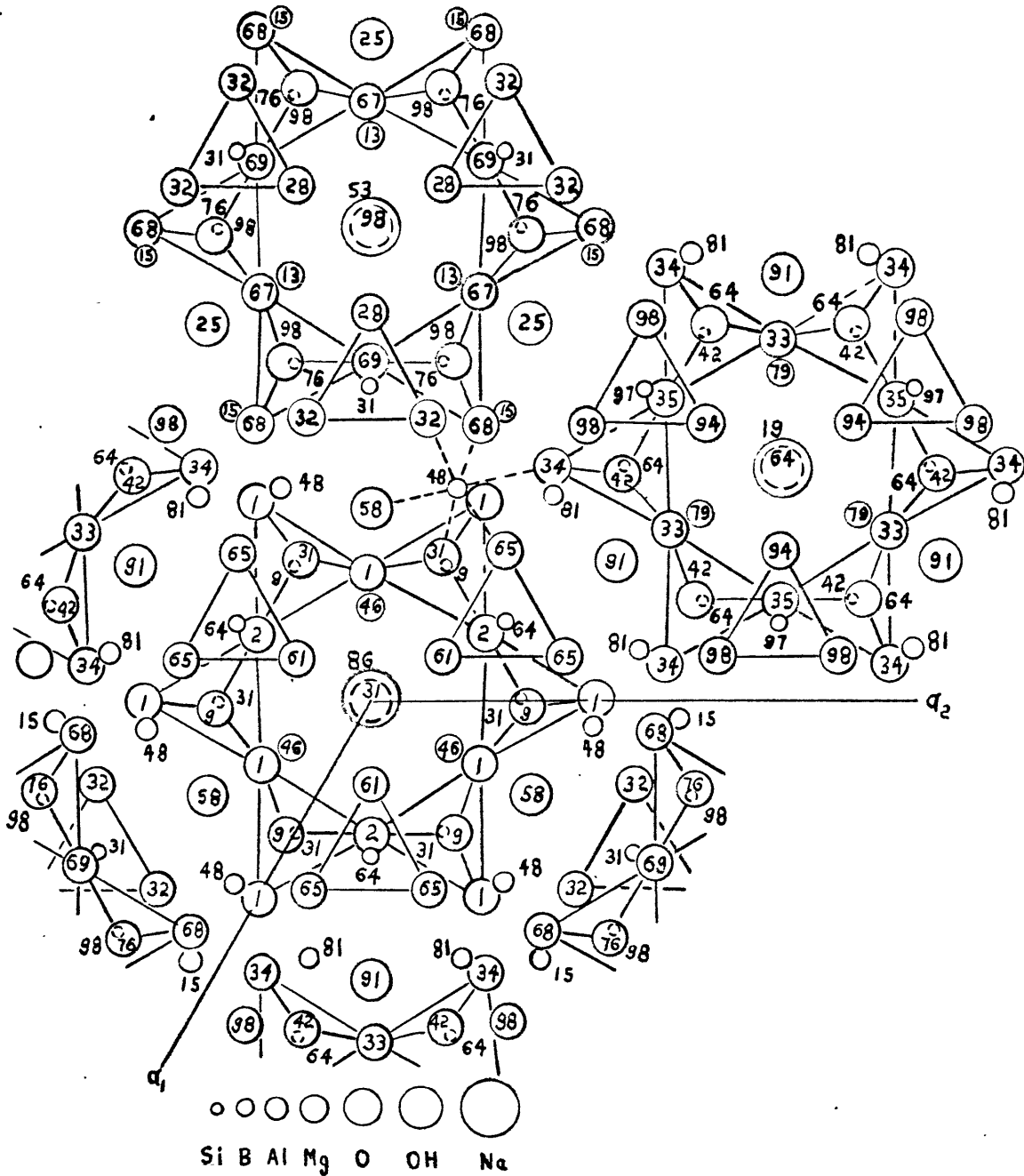


Figure 1. The structure of tourmaline, $\text{NaMg}_3\text{Al}_6(\text{BO}_3)_3\text{Si}_6\text{O}_{18}(\text{OH})_4$. BO_3 triangles and SiO_4 tetrahedra in the $\text{Si}_6\text{O}_{18}(\text{OH})_4$ rings are outlined. The octahedral binding of an Al atom is indicated by broken lines. (after Ito and Sadanaga, 1951). The diagram shows the fractional height of each ion along the c - axis.

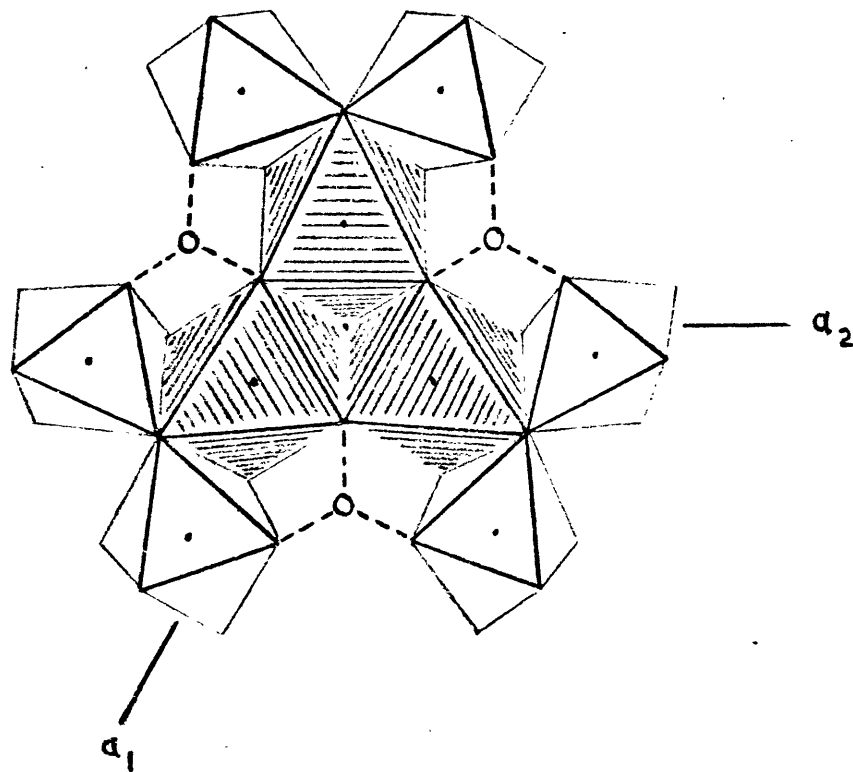


Figure 2. The upper layer of the tourmaline structure chiefly consists of octahedra. The central three, larger octahedra contain the Y cations. The six, smaller, peripheral octahedra contain the Z cations. The small circles are B atoms bonded along the broken lines to the corners of octahedra. (after Buerger, 1962).

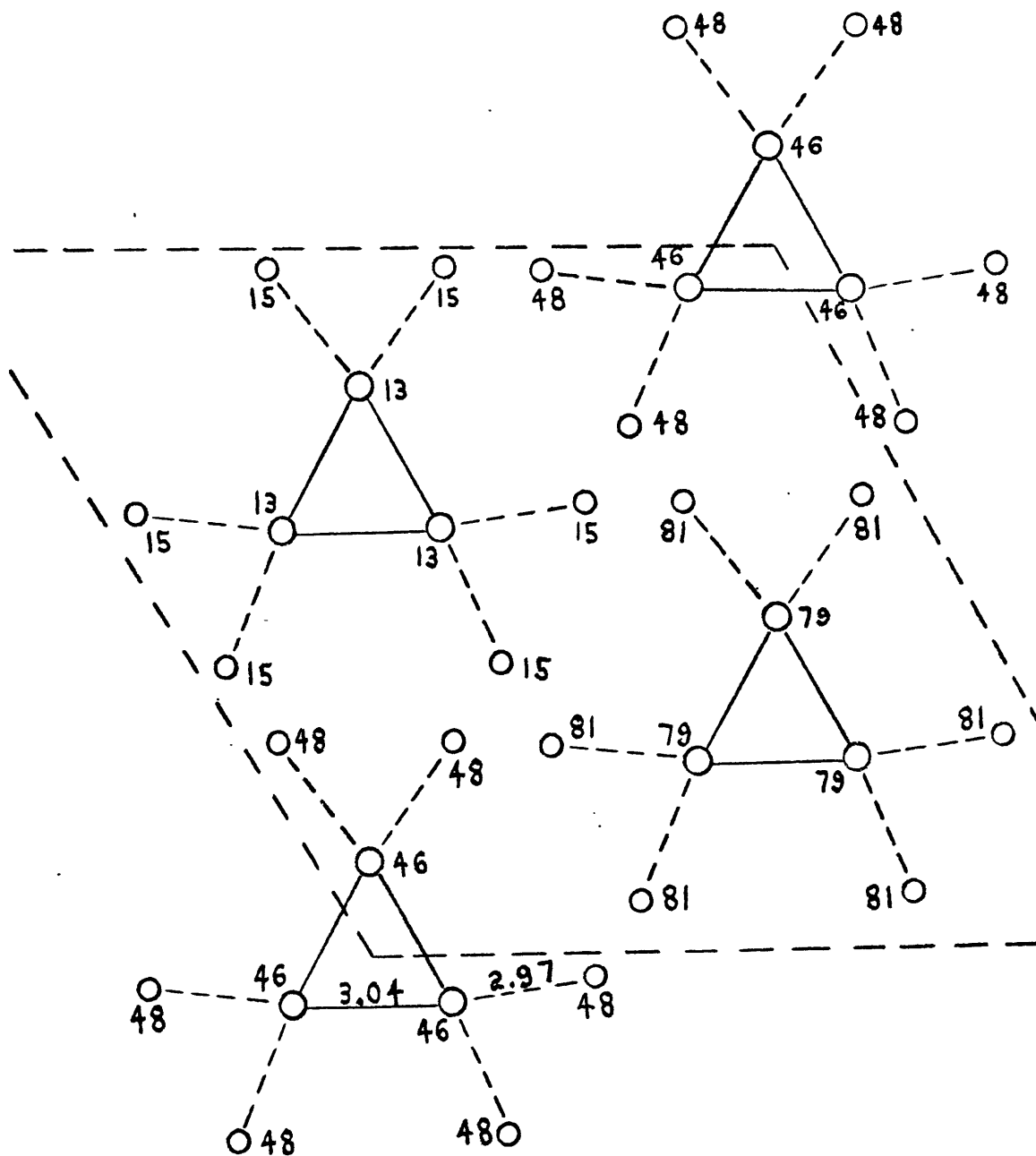
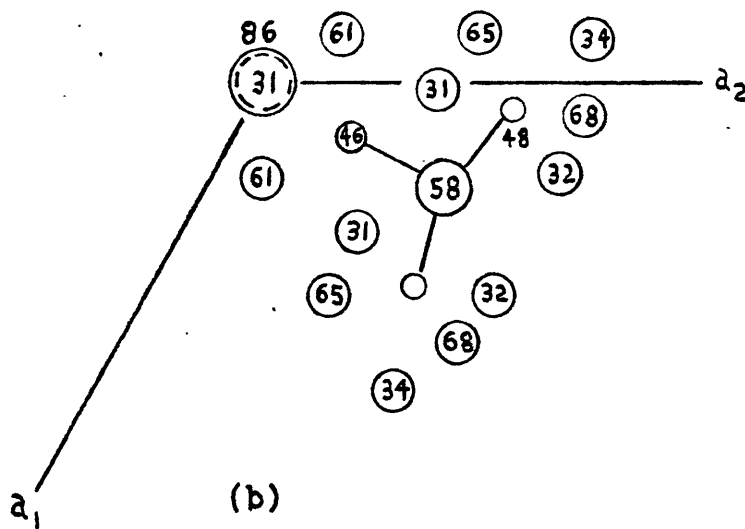
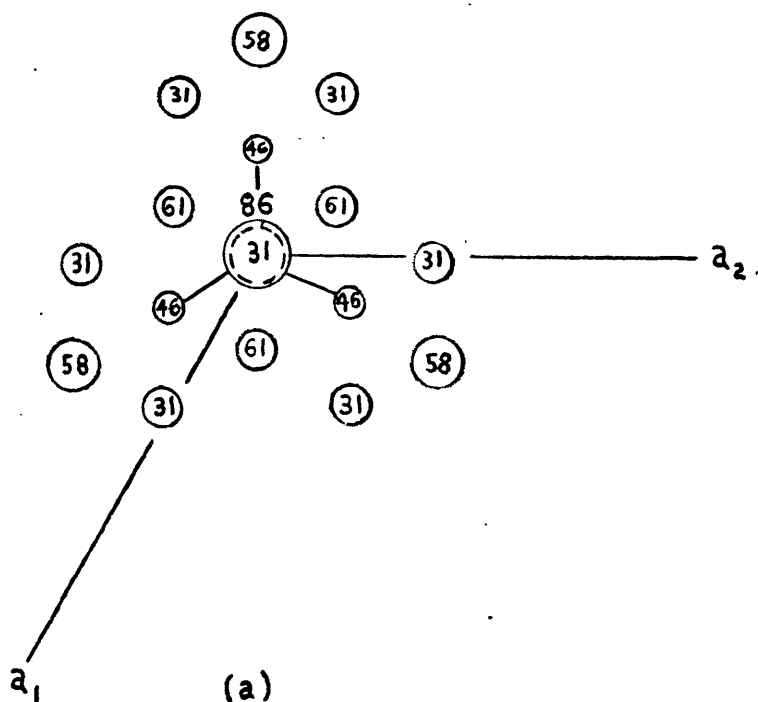


Figure 3. A (001) projection showing the locations of nearest neighbor cations in edge-shared octahedra. The diagram shows the fractional height of each cation along the c - axis, and the metal-metal distances (in Å). (after Faye, 1968).

- (Brown) - Y cations in the 9 (b) position.
- (Green) - Z cations in the 18(c) position.



○ ○ ○ ○ ○
Al Mg O OH Na

Figure 4. Cation co-ordination with the hydroxyl ions in the tourmaline structure.

- (a) The O_1 (OH_I) site with three Y and one X nearest neighbors.
- (b) The O_3 (OH_{II}) site with one Y and two Z nearest neighbors.

○ (Brown) - Y cations in the 9(b) position.
○ (Green) - Z cations in the 18(c) position.

Chapter 3

EXPERIMENTAL

3.1 Cell Dimensions

The specimens analyzed in this study are summarized in Table 1. Cell dimensions were determined by the use of a Norelco, X-ray, powder diffractometer, using a cobalt source ($\lambda K_{\alpha} = 1.78890\text{\AA}$) with a nickel filter. Four passes were made at room temperature, two from 15° to 80° and two in the reverse direction. Averaged 2θ values were obtained after standardizing each pattern relative to an internal KBr diffraction pattern. Cell parameters were then calculated from the derived "d" spacings using the "Least Squares Fit for Cell Parameters" computer program, written by D.E. Appleman. The final values are tabulated in Table 1 and plotted in Table 2.

Samples were prepared by finely grinding the mineral and spreading it on a glass slide, using acetone as a wetting and binding agent.

3.2 Chemical Analysis

Partial chemical analyses were accomplished by the Automated MAC 5 electron microprobe, using the GEOLAB analysis system. All major elements above atomic number ten were analyzed, with the results summarized in Table 3. Chemical compositions are given in weight percents of oxides, and formulae are expressed in terms of six silicon atoms per formula unit.

Table 1. Tourmaline Specimens with Cell Parameters.

No.	Sample	a	c	c/a	10^{-6} m.
1.	Red(Rubellite)(Manjaka, Madagascar)*	15.800	7.079	0.4480	240
2.	Pink(Mt. Mica, Maine) 108916 *@	15.845	7.103	0.4483	242
3.	Pale Green(Mt. Mica, Maine) 108913 *@	15.865	7.103	0.4477	174
4.	Black(Cornwall, England) R3963 (USNM)	15.896	7.107	0.4471	110
5.	Pale Blue(Mt. Mica, Maine) 108912 *@	15.908	7.122	0.4477	176
6.	Green(Governador, Minas Geras, Brazil) 97723 *@	15.914	7.128	0.4479	166
7.	Black(Locality Unknown) 108914 *@	15.965	7.198	0.4509	110
8.	Brown(Brazil) 86330 *@	15.946	7.213	0.4523	228
9.	Blue(Goshen, Mass.) 895 *	15.910	7.186	0.4517	80
10.	Pale Blue(No. 5 heated) 108912 *@	15.838	7.135	0.4505	176
11.	Pale Cream(DeKalb, N.Y.) 86321 *	15.924	7.205	0.4525	326
12.	Green(Chromium) *	15.931	7.195	0.4516	246

* Harvard Museum Number.

@ Samples used by Wilkins et al., 1969.

Table 2. Cell Parameters (a vs. c) of the Tourmaline Specimens used in This Study.

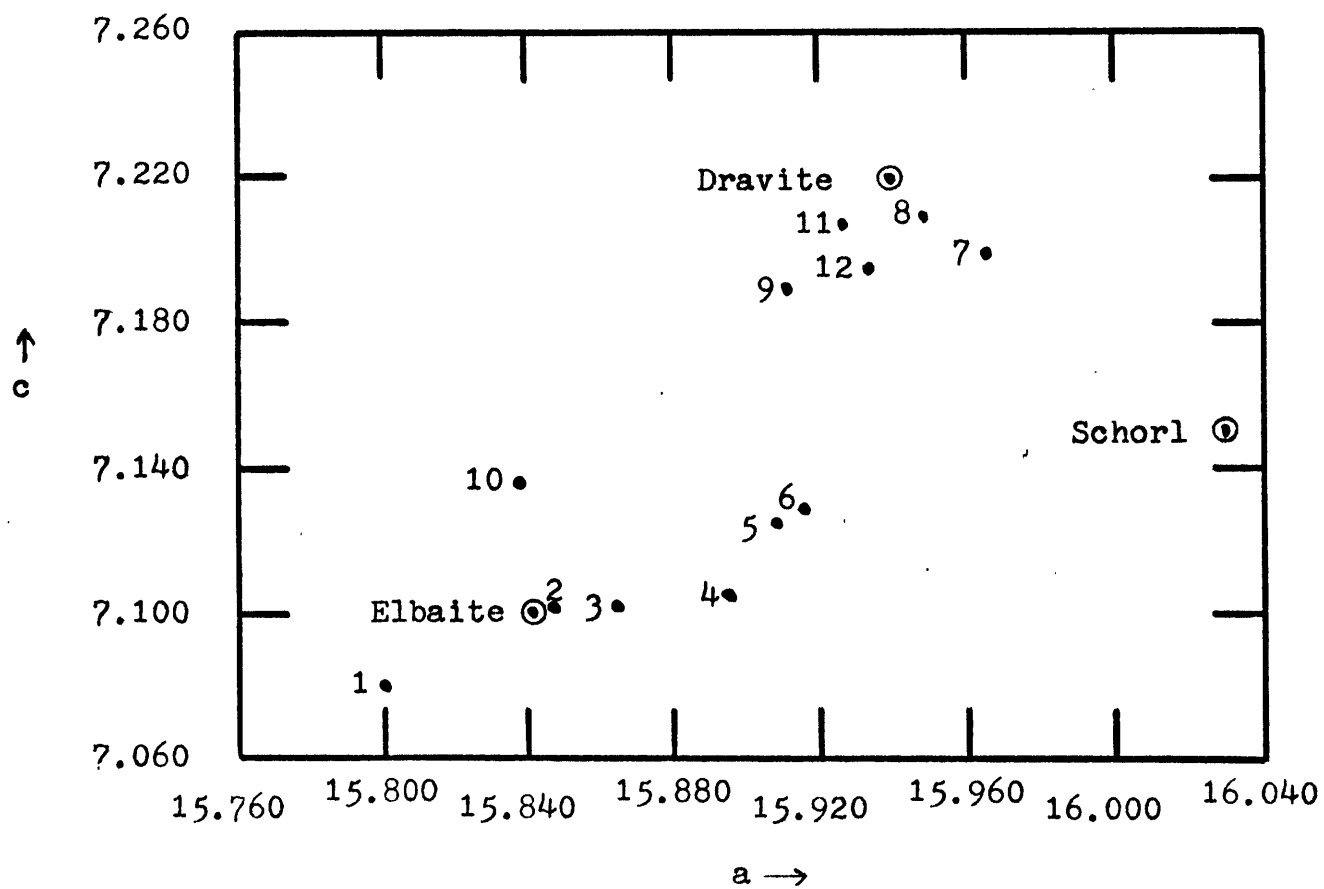


Table 3. Chemical Analyses of Tourmalines. Figures are in Weight Percents of Oxides. Chemical Formulae are Normalized to Si = 6.000 *

	1	2	3	4	5	6	7@	8	9	10@	11	12
SiO ₂	36.35	38.36	38.00	37.31	37.19	37.33	37.05	38.14	35.73	37.80		37.64
TiO ₂	0.07	0.05	0.09	0.22	0.10	0.64	0.16	1.04	0.54	0.07		0.74
Al ₂ O ₃	45.84	43.23	41.49	38.79	38.19	35.23	30.63	29.14	34.50	38.01		32.52
Fe ₂ O ₃	0.04	0.09	2.09	5.77	6.70	6.57		0.84	8.33		(Cr ₂ O ₃)	0.38
FeO							9.81			6.53		
MnO	0.54	0.98	1.47	0.02	0.55	0.04	0.11	tr	0.01	0.73		tr
MgO	0.20	0.15	0.20	0.77	0.18	3.39	6.02	14.82	5.51	0.16		12.04
CaO	0.42	0.47	0.36	0.10	0.10	0.05	0.39	1.74	0.36	0.10		2.26
Na ₂ O	2.19	2.00	2.61	2.01	2.84	2.69	2.08	1.02	2.38	2.51		1.60
K ₂ O	0.02	0.03	0.02	0.01	0.02	0.03	0.02	0.06	0.03	0.04		0.10
Total	85.67	85.36	86.33	85.00	85.87	85.97	86.37	86.80	87.39	85.95		87.28
Si	6.000	6.000	6.000	6.000	6.000	6.000	6.000	6.000	6.000	6.000	5.580	6.000
Ti	0.009	0.006	0.010	0.027	0.013	0.077	0.019	0.123	0.069	0.009	tr	0.089
Al	8.918	7.970	7.721	7.351	7.262	6.673	5.846	5.403	6.828	7.111	5.580	6.109
Fe ³⁺							1.319			0.867	(Cr)	0.048
Fe ²⁺	0.006	0.012	0.276	0.776	0.904	0.883		0.111	1.169		0.030	0.000
Mn	0.075	0.130	0.196	0.003	0.076	0.006	0.016	tr	0.001	0.098	tr	tr
Mg	0.050	0.035	0.047	0.185	0.044	0.812	1.453	3.474	1.379	0.038	3.550	2.861
Ca	0.074	0.079	0.061	0.017	0.017	0.009	0.068	0.293	0.065	0.017	0.600	0.386
Na	0.700	0.607	0.799	0.626	0.888	0.838	0.654	0.312	0.775	0.773	0.390	0.494
K	0.004	0.006	0.004	0.002	0.004	0.006	0.004	0.011	0.006	0.008	0.010	0.021

* Except #11 (from Buerger et al., 1962)

@ Distinction between Fe²⁺ and Fe³⁺ could not be resolved in microprobe analysis.

Specimens were prepared by cementing small pieces of the mineral, using epoxy resin, into holes drilled in two, 1-inch diameter discs. The discs were then ground, and finally polished with 0.3 micron alpha alumina powder. The exposed, polished crystal surfaces were electrocoated with carbon to give a positive ground for the electron beam.

3.3 Mössbauer Spectroscopy

The Mössbauer spectra were obtained from a spectrometer designed by Austin Science Associates operating in the constant acceleration, symmetric, sawtooth velocity mode. A 100 mc ^{57}Co on palladium matrix was the source of gamma rays, and the spectra were accumulated in 512 channels of a Nuclear Data multi-channel analyzer.

Absorbers were prepared by mixing the powdered mineral with the same volume of sucrose, grinding the mixture, and sprinkling the powder into a plexiglass disc. This technique has proved to be effective for overcoming asymmetry effects due to preferred orientation of the crystallites (Burns and Greaves, 1971). Although tourmalines have no cleavage, so that effects of preferred orientation are reduced, nevertheless the "sugar technique" was adopted in this study to eliminate asymmetry effects in the Mössbauer spectra (Burns, 1972).

All spectra were recorded with the mineral samples held at room temperature. The program written by Stone et al., 1971, entitled "General Constrained Non-linear Regression for Mössbauer

Spectra", was used to fit Lorentzian curves to the experimental data. Calibrations of the isomer shifts were made relative to the spectrum of a metallic iron foil standard. Computer Lorentzian curve fits were initially fully constrained, in pairs, for widths and intensities. Successive stages of convergence were obtained by releasing constraints until the program either diverged in its fitting process or became fully unconstrained. Mössbauer parameters for each stage fitted to experimental data are summarized in Tables 4 and 5. Mössbauer spectra, with constraints indicated on each spectrum, are presented in Figures 5 through 12.

3.4 Optical/Near-infrared Spectroscopy

The optical/near-infrared absorption spectra for all samples were measured on a Cary model 17 ratio recording spectrophotometer employing polarizing microscopes in the light paths (Burns, 1966). Single, thin sectioned, crystals of the minerals, oriented with the c-axis \perp to the light beam, were mounted on glass slides and placed on the flat stage of the microscope containing calcite Nicol polarizers. A second microscope holding only a glass slide was inserted in the reference beam and also placed in the light tight compartment between light source and detectors of the spectrophotometer (Burns, 1972).

The relatively large single crystals of the tourmalines, being uniaxial, were simply cut parallel to the c-axis with a diamond edged saw. The resulting sections were mounted on glass

slides and ground to micro-thicknesses indicated in Table 1, for the measurement of the desired spectra (Faye et al., 1968).

The chart output from the Cary 17 [absorption units vs. nanometers (10^{-9} m)] were replotted as absorption units vs. energy units (cm^{-1}). These spectra were broken down into their component Gaussian curves, employing the use of a Dupont 310 Curve Resolver. Fitted component Gaussian curves, with their absorption spectra envelopes, are presented in Figures 13 through 21.

3.5 First-overtone, O-H Bond, Stretch Spectra

The first-overtone, O-H bond, stretch spectra were obtained by the same method as the absorption spectra. Replotting in absorption vs. energy units was not undertaken since the limits of pertinent data were very narrow (100 nm). The spectrum of specimen #11, a magnesia tourmaline approximating the ideal dravite composition, was fitted with six component Gaussian curves and is included as Figure 22. All other O-H bond, stretch spectra are presented according to their enrichment in iron or magnesium, and are summarized in composite Figures 23 and 24.

Table 4. Mossbauer Parameters for the Fe²⁺ - Fe³⁺ Tourmalines. @

Sample	Peaks	Q.S. (mm/sec)	C.S. (mm/sec)	5 Constraints		
				H.W. (mm/sec)	A. Ratio	χ^2
3.	Outer	2.37	1.11	0.39	6.706	582
	Inner	2.02	1.11	0.39	1	
4.	Outer	2.32	1.05	0.38	7.474	615
	Inner	1.56	1.00	0.38	1	
5.	Outer	2.41	1.11	0.42	4.816	692
	Inner	2.12	1.11	0.42	1	
6.	Outer	2.38	1.08	0.42	4.625	791
	Inner	1.41	1.08	0.42	1	
8.	Outer	2.32	1.09	0.42	1.988	514
	Inner	1.52	1.12	0.42	1	
9.	Outer	2.38	1.05	0.41	4.530	1289
	Inner	1.88	1.05	0.41	1	
				7 Constraints		
10.	Outer	2.39	1.03	0.31	1.585	633
	Fe ²⁺ -Inner	2.08	0.97	0.46	4.354	
	Fe ³⁺ -Inner	0.55	0.52	0.85	1	
7.	Outer	2.43	1.06	0.33	1.882	1310
	Fe ²⁺ -Inner	1.73	0.93	0.61	1.037	
	Fe ³⁺ -Inner	0.79	0.53	0.70	1	

@ Spectra measured at room temperature. C.S. shift is relative to metallic iron.

Table 5. Continuation of Mossbauer Parameters for the Fe²⁺ - Fe³⁺ Tourmalines.

Sample	Peaks	4 Constraints			3 Constraints			1 Constraint		
		H.W. (mm/sec)	A. Ratio	X ²	H.W. (mm/sec)	A. Ratio	X ²	H.W. (mm/sec)	A. Ratio	X ²
3.	Outer Inner	0.38 0.38	3.220 1	580	0.38 0.46	4.998 1	578	Process Diverged		
4.	Outer Inner	0.38 0.38	7.255 1	591	0.35 0.66	3.216 1	551	0.35 0.60	3.392 1	550
5.	Outer Inner	0.42 0.42	7.569 1	685	0.38 0.38	1.337 1	610	Process Diverged		
6.	Outer Inner	0.42 0.42	4.614 1	754	0.40 0.52	3.538 1	710	0.40 0.47	3.580 1	680
8.	Outer Inner	0.42 0.42	2.026 1	510	0.40 0.44	1.800 1	509	0.37 0.44	1.770 1	505
9.	Outer Inner	0.41 0.41	4.525 1	1267	0.34 0.65	1.303 1	819	0.34 0.67	1.311 1	815
		5 Constraints			4 Constraints			3 Constraints		
10.	Outer Fe ²⁺ -Inner Fe ³⁺ -Inner	No Data			0.36 0.48 0.70	4.750 2.035 1	586	No Data		
7.	Outer Fe ²⁺ -Inner Fe ³⁺ -Inner	Process Diverged								

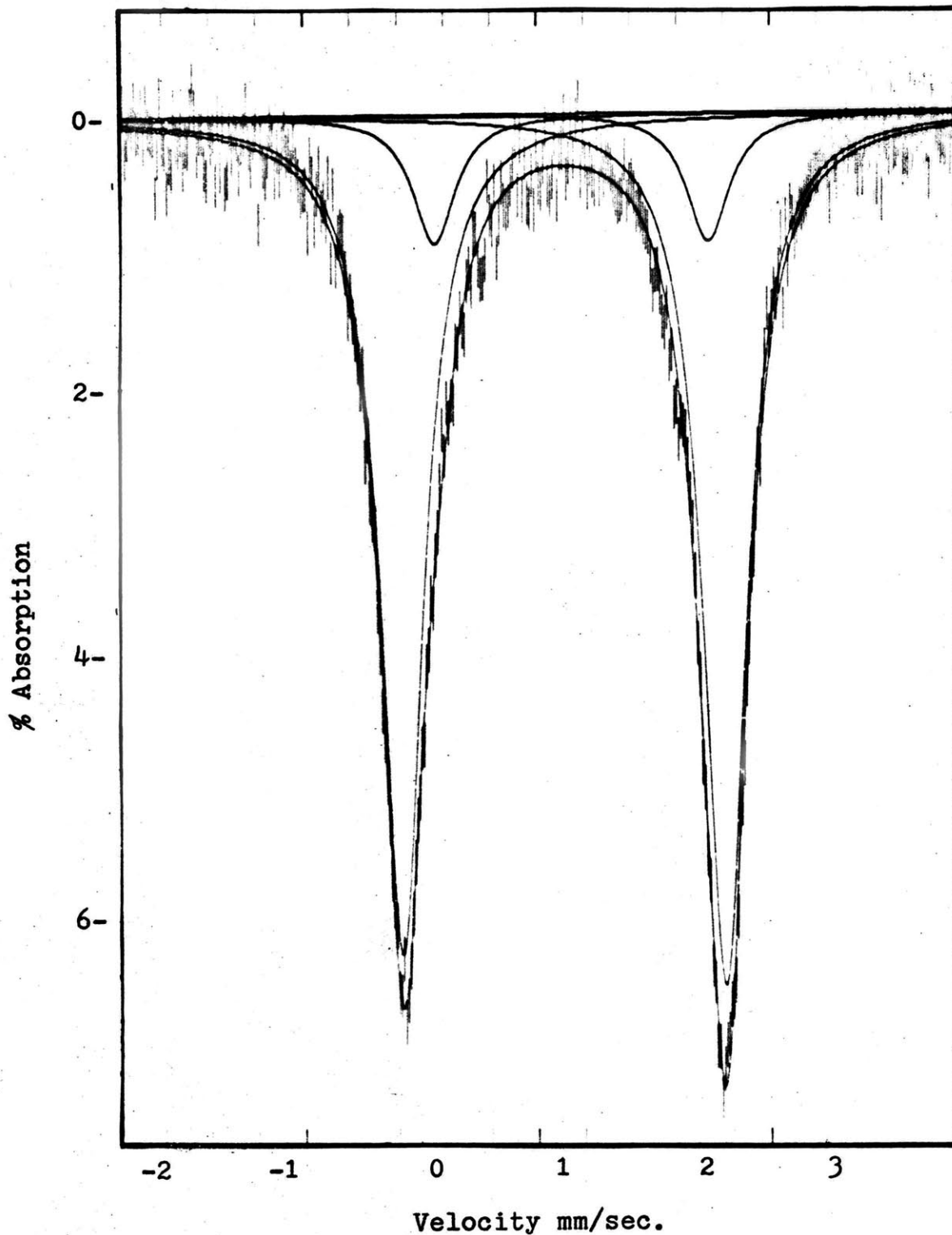


Figure 5. Mössbauer spectrum of tourmaline #3. The spectrum has been fitted to two ferrous doublets, with halfwidths and intensities constrained in pairs.

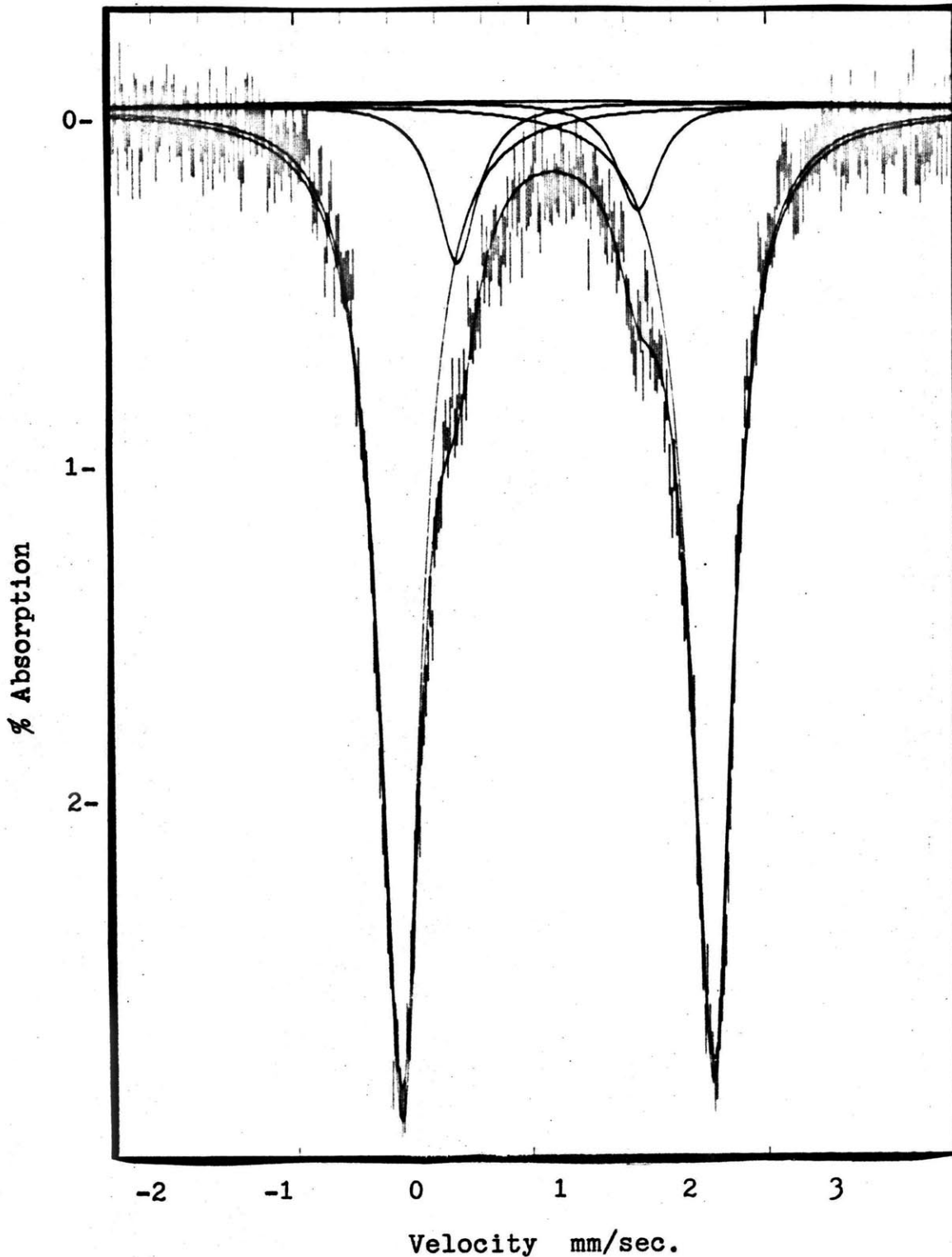


Figure 6. Mossbauer spectrum of tourmaline #4. The spectrum has been fitted to two ferrous doublets, with halfwidths constrained in pairs.

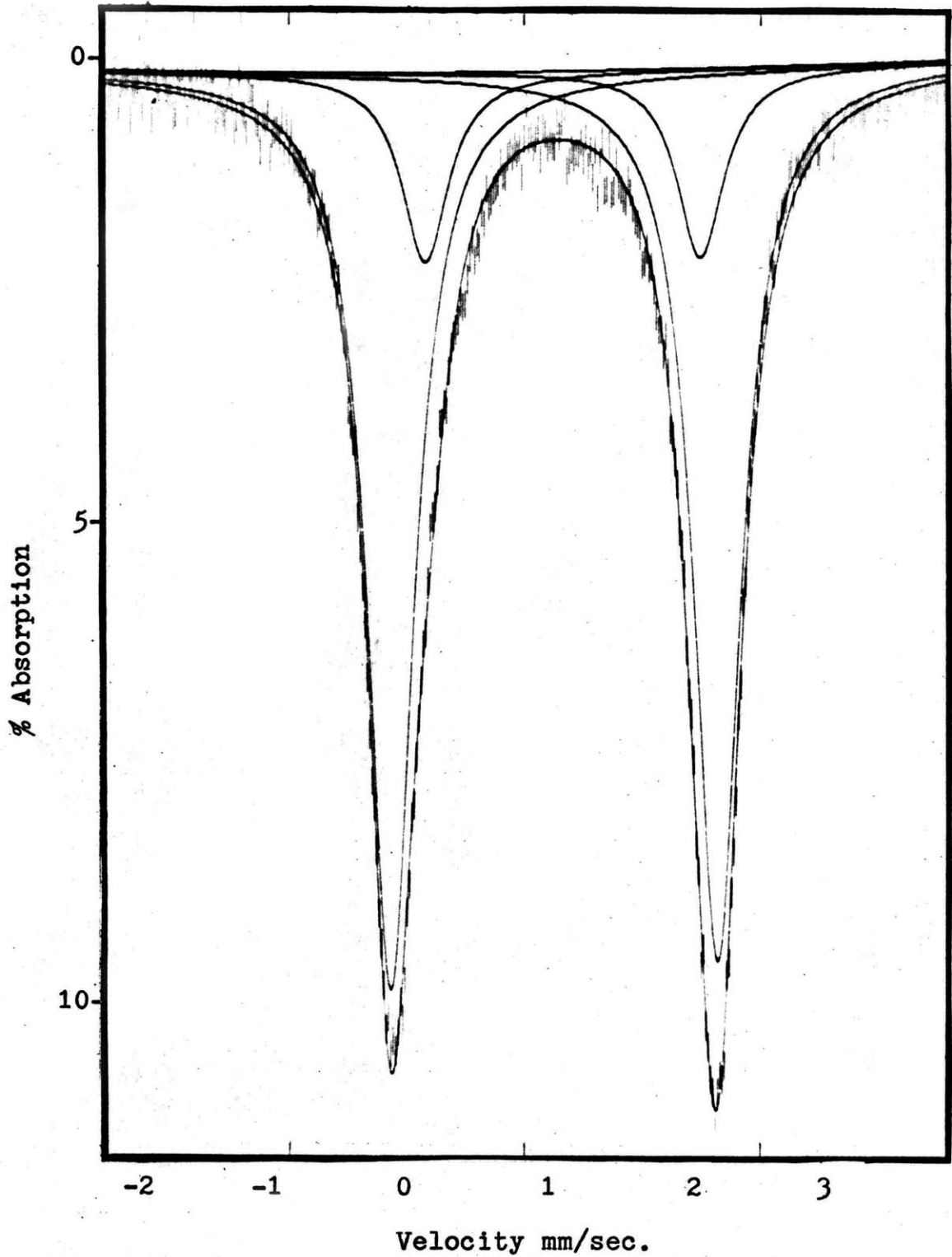


Figure 7. Mossbauer spectrum of tourmaline #5. The spectrum has been fitted to two ferrous doublets, with halfwidths and intensities constrained in pairs.

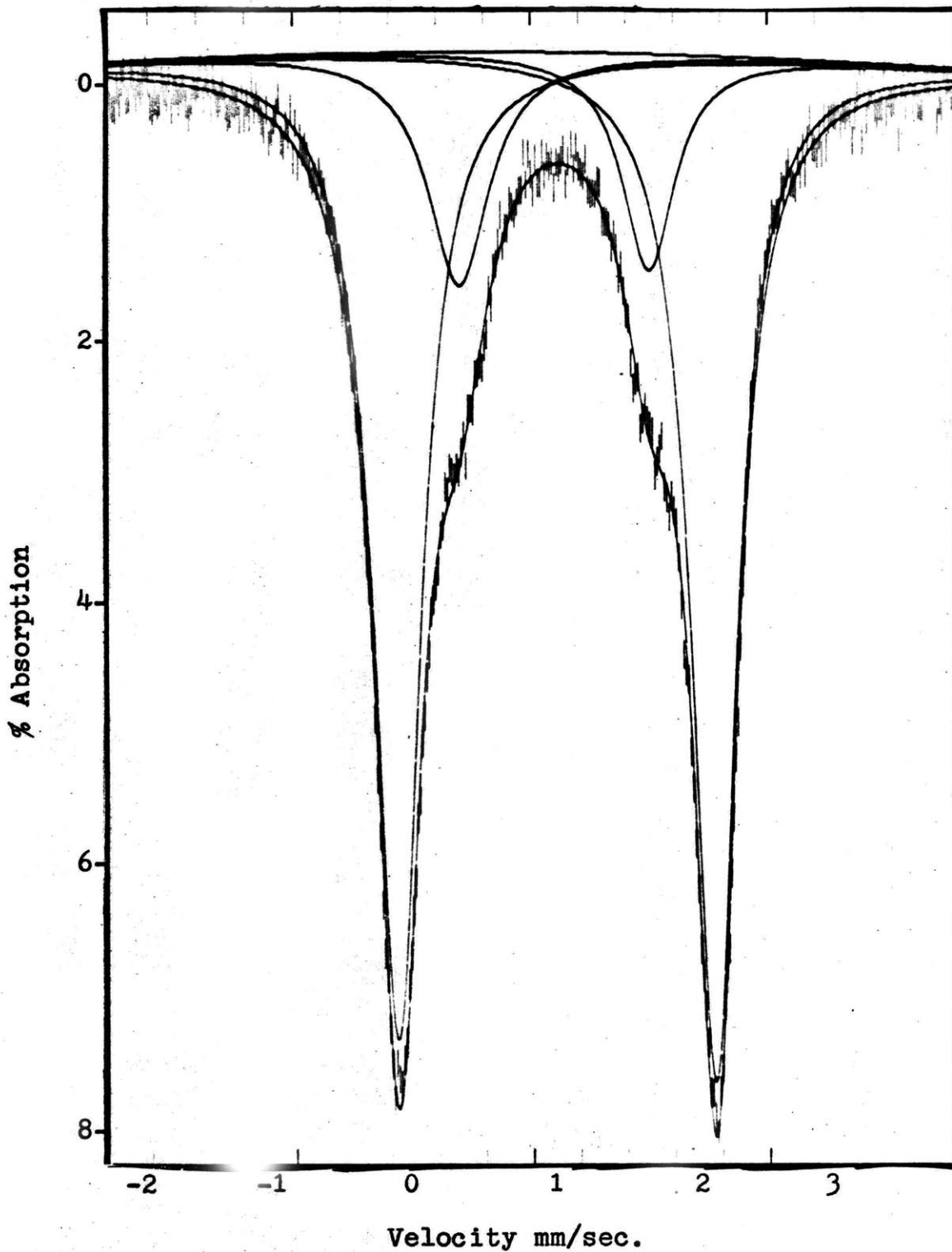


Figure 8. Mossbauer spectrum of tourmaline #6. The spectrum has been fitted to two ferrous doublets, with no constraints in pairs.

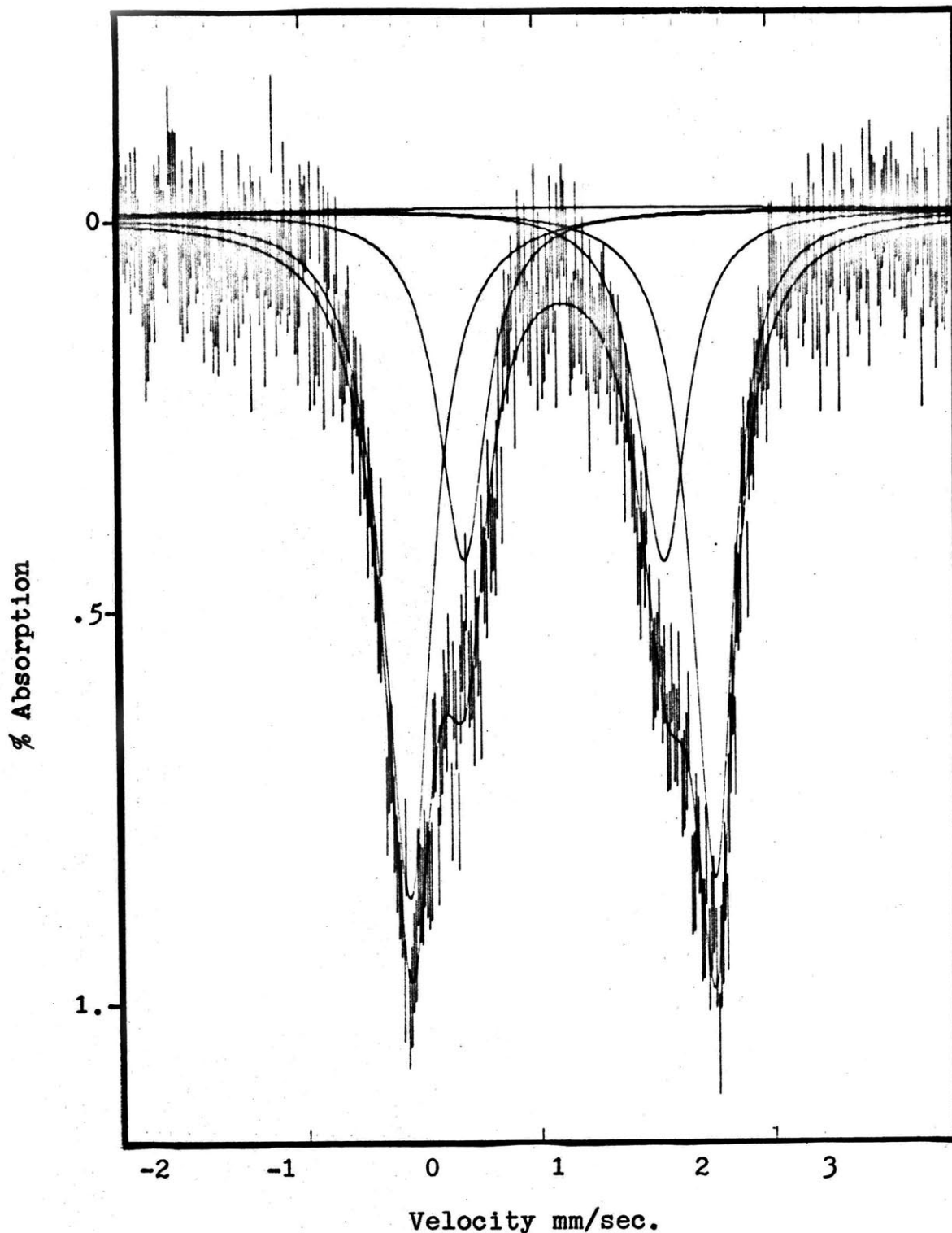


Figure 9. ⁵⁷Fe Mössbauer spectrum of tourmaline #8. The spectrum has been fitted to two ferrous doublets, with no constraints in pairs.

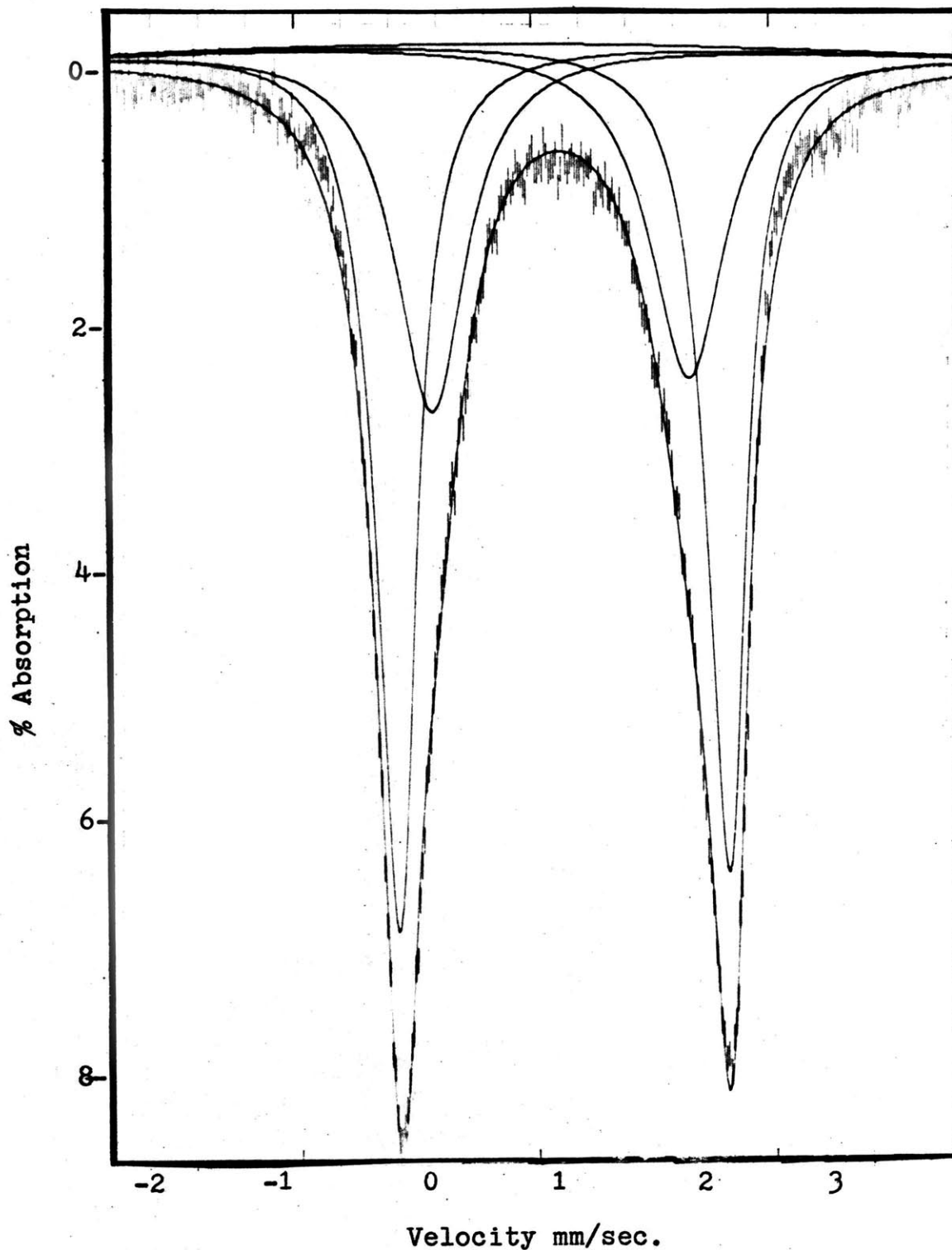


Figure 10. Mossbauer spectrum of tourmaline #9. The spectrum has been fitted to two ferrous doublets, with halfwidths constrained in pairs.

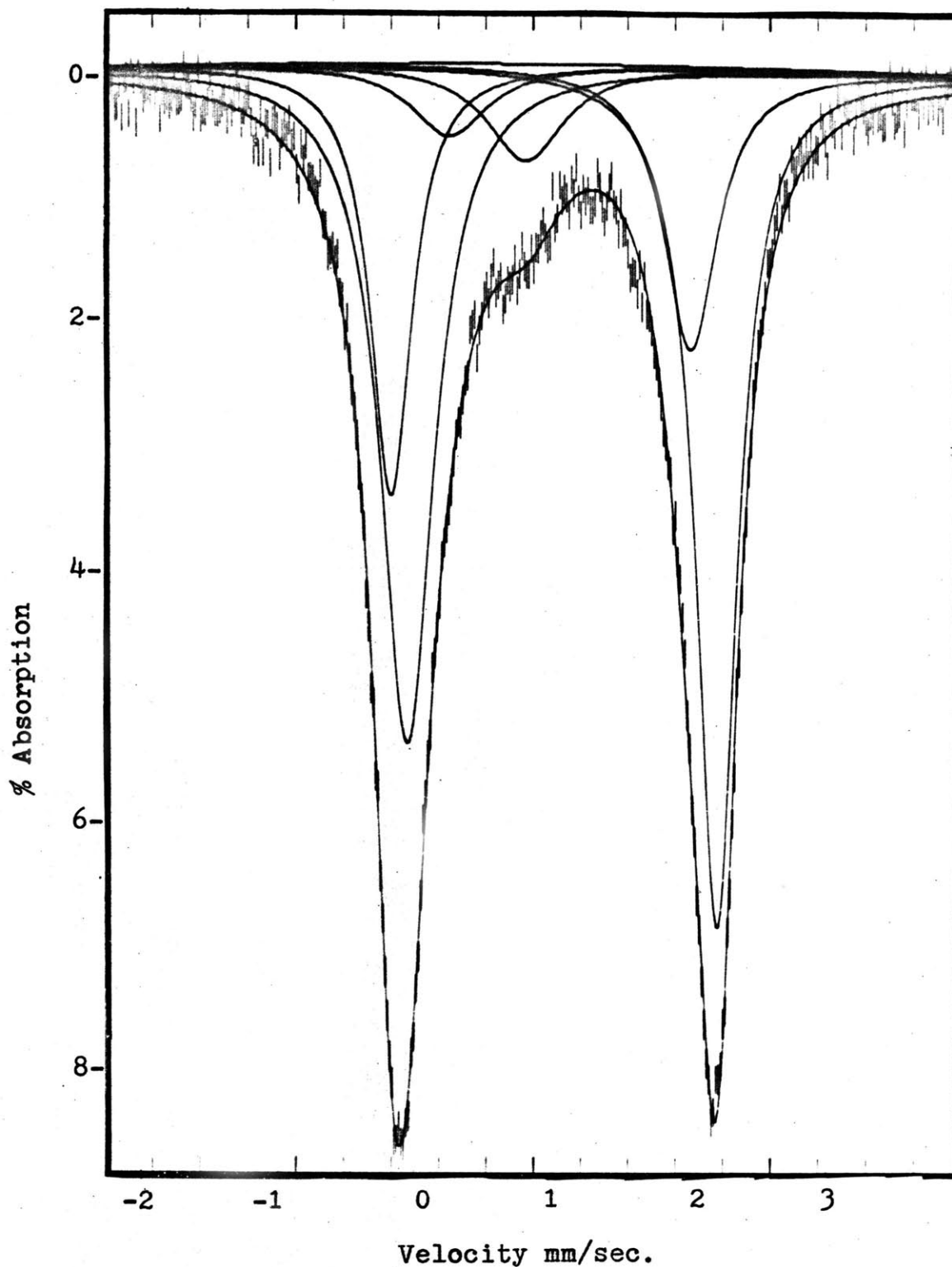


Figure 11. ⁵⁷Fe Mössbauer spectrum of tourmaline #10. The spectrum has been fitted to two ferrous and one ferric, doublets, with halfwidths constrained in pairs.

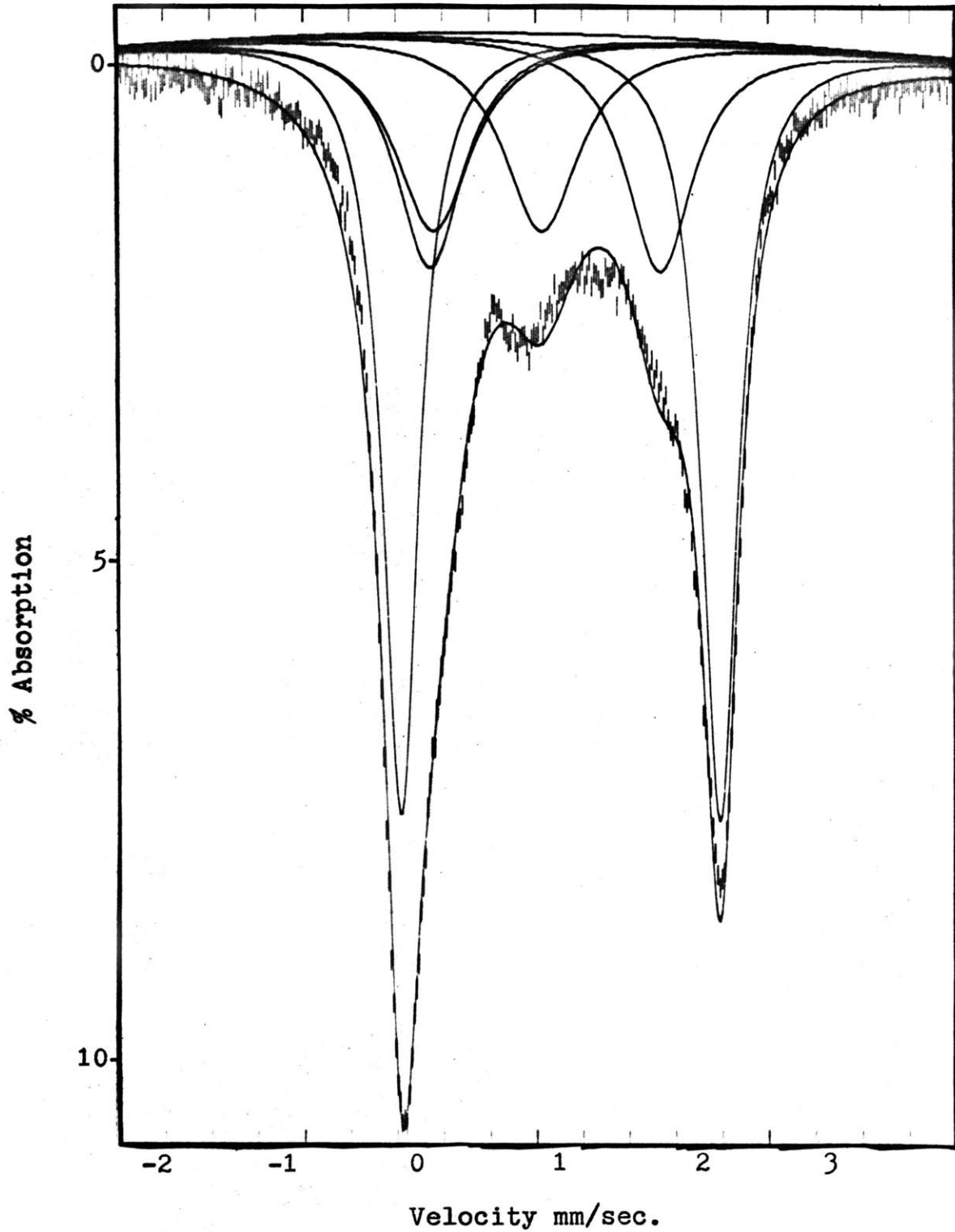


Figure 12. ⁵⁷Fe Mössbauer spectrum of tourmaline #7. The spectrum has been fitted to two ferrous and one ferric, doublets, with halfwidths and intensities constrained in pairs.

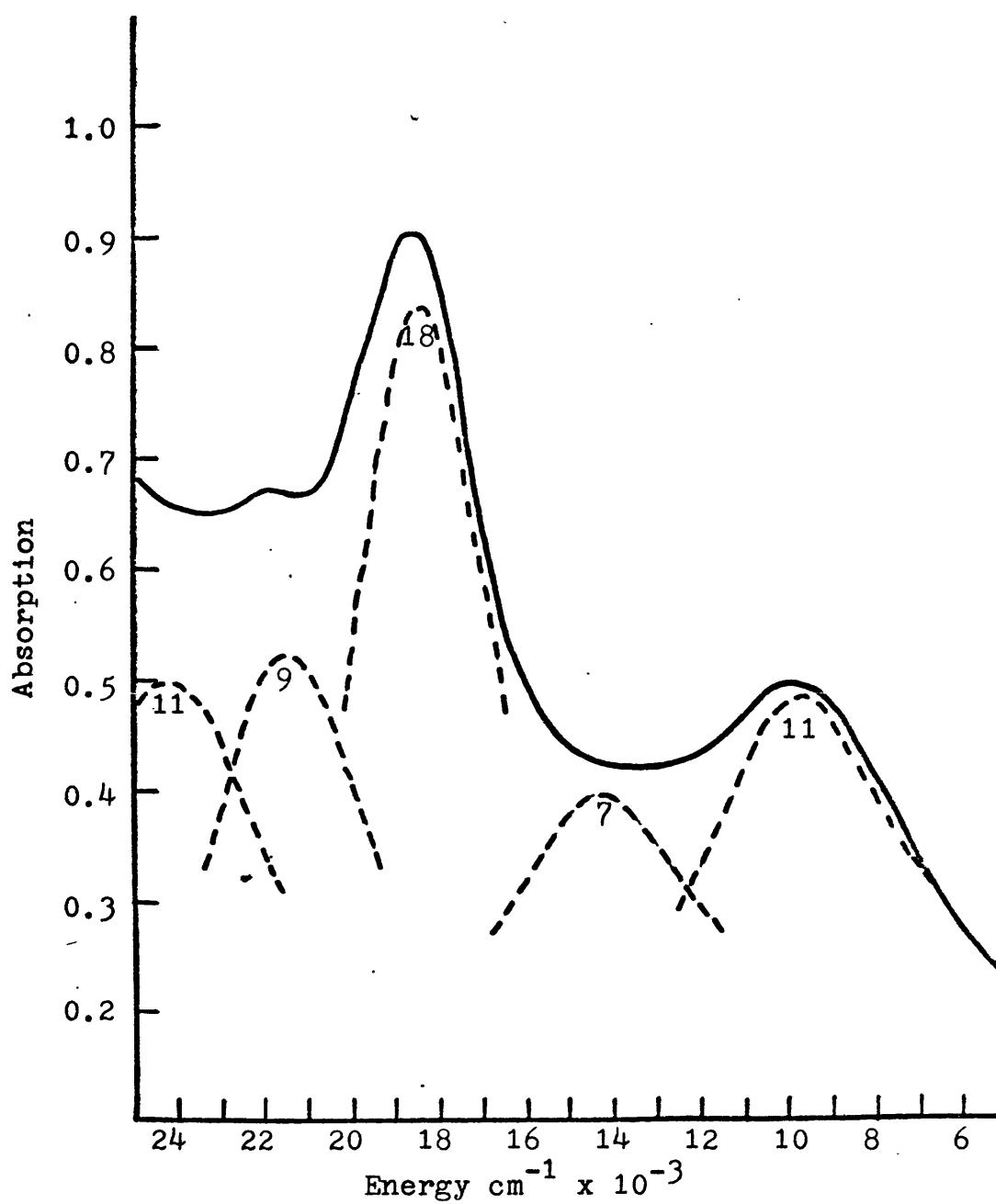


Figure 13. Polarized absorption spectrum of tourmaline #1. The figure shows the EIC spectrum fitted to component gaussian peaks, with percentage area of each peak.

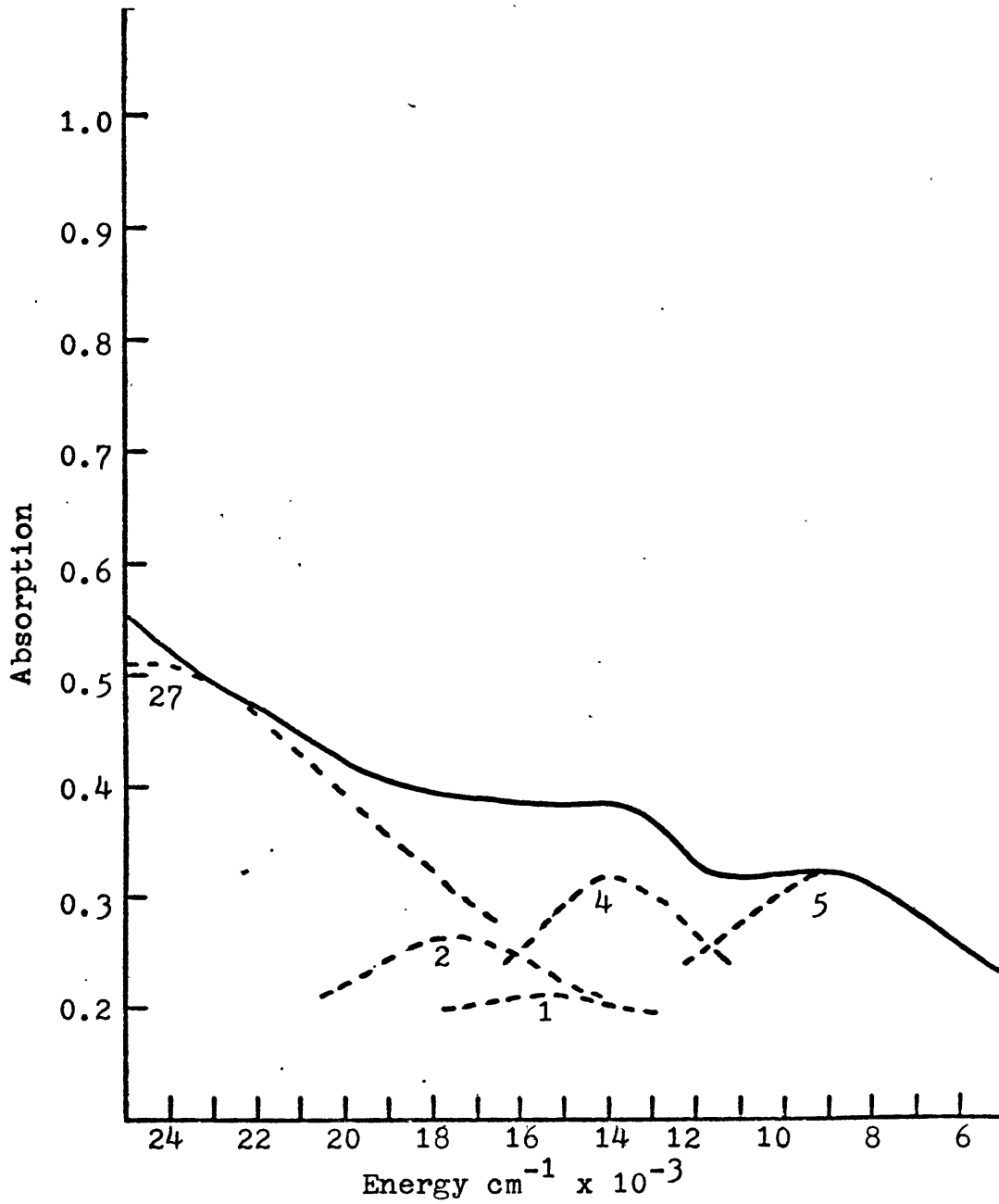


Figure 14. Polarized absorption spectrum of tourmaline #3. The figure shows the ELC spectrum fitted to component gaussian peaks, with percentage area of each peak.

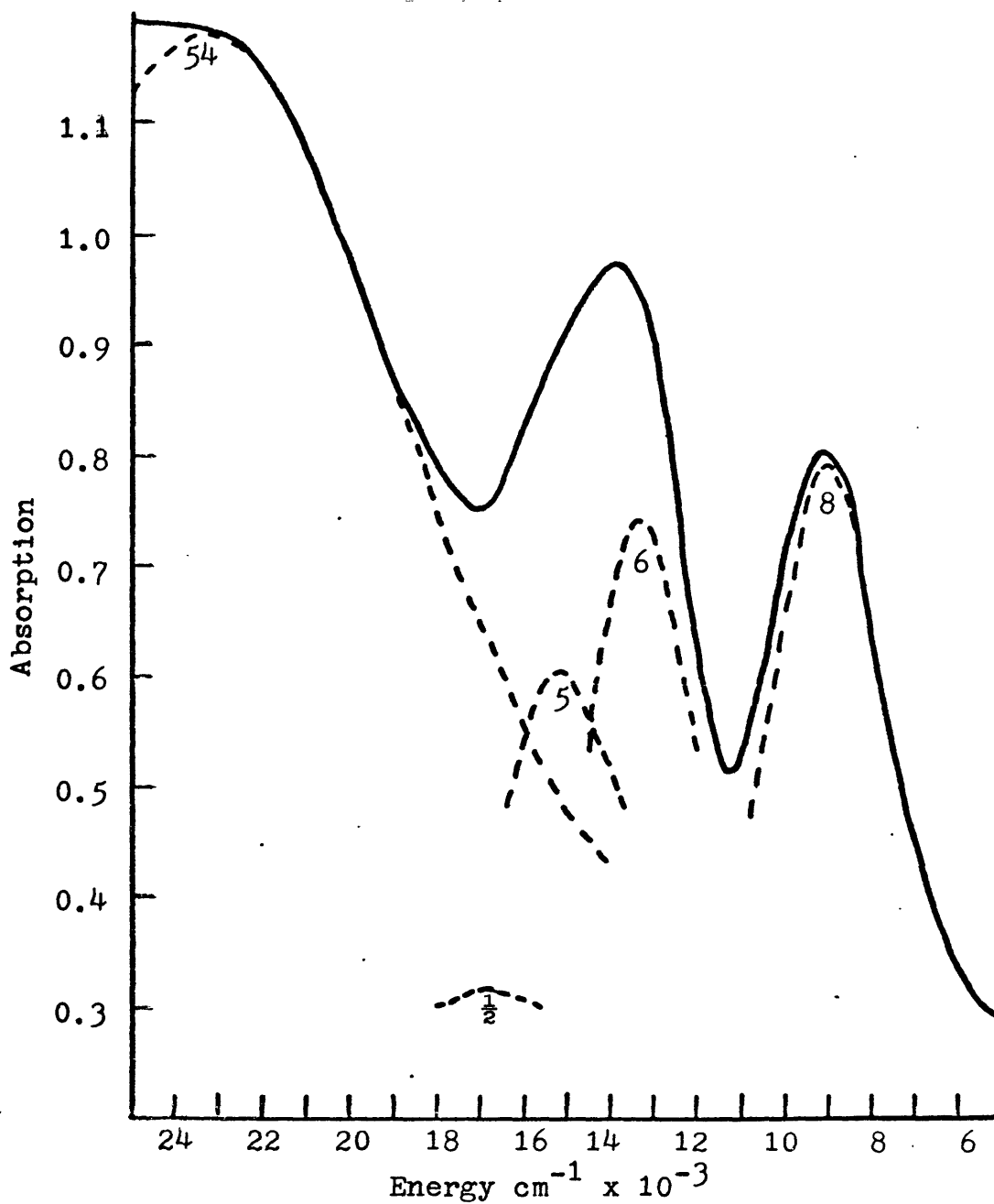


Figure 15. Polarized absorption spectrum of tourmaline #4. The figure shows the ELC spectrum fitted to component gaussian peaks, with percentage area of each peak.

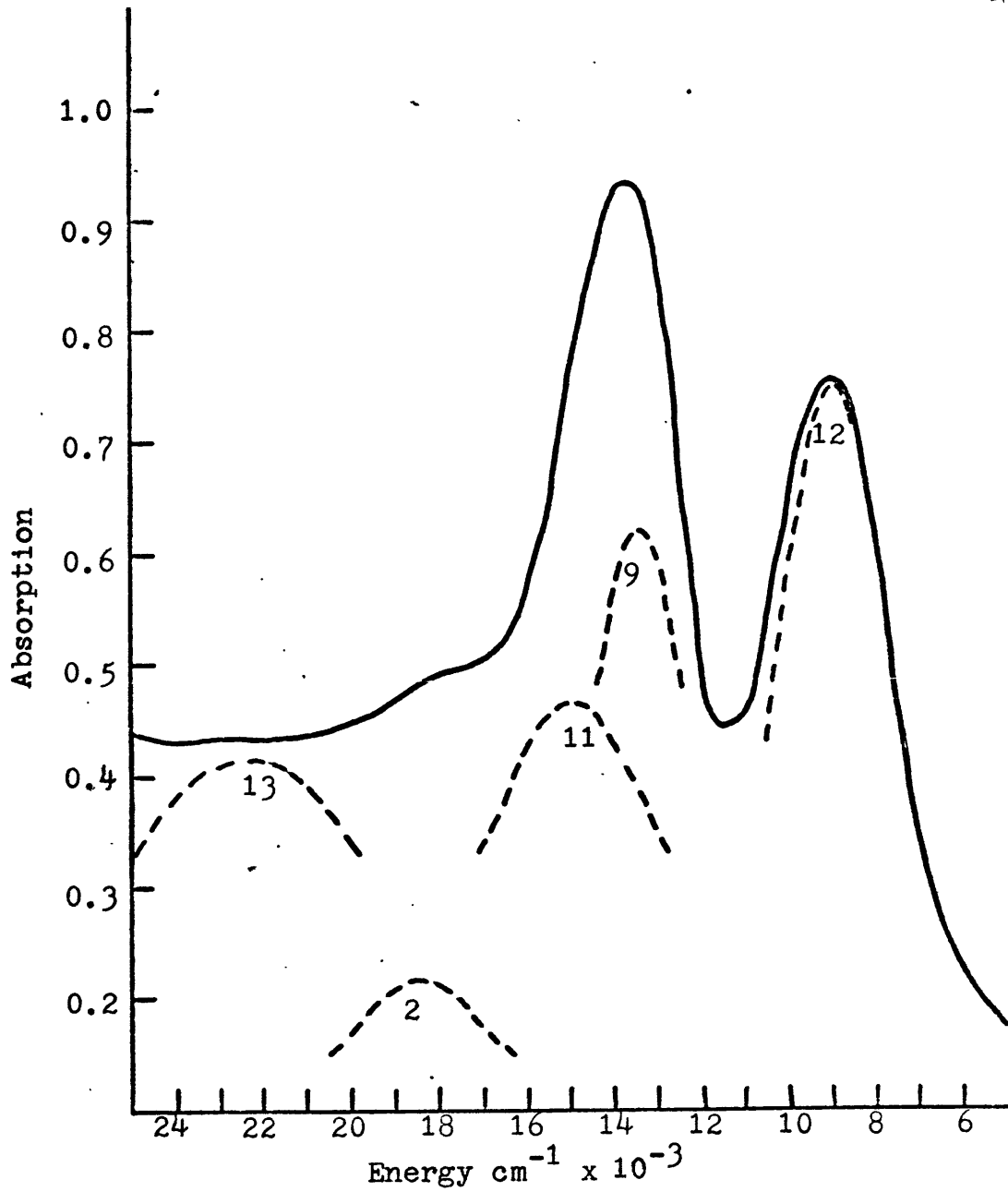


Figure 16. Polarized absorption spectrum of tourmaline #5. The figure shows the EIC spectrum fitted to component gaussian peaks, with percentage area of each peak.

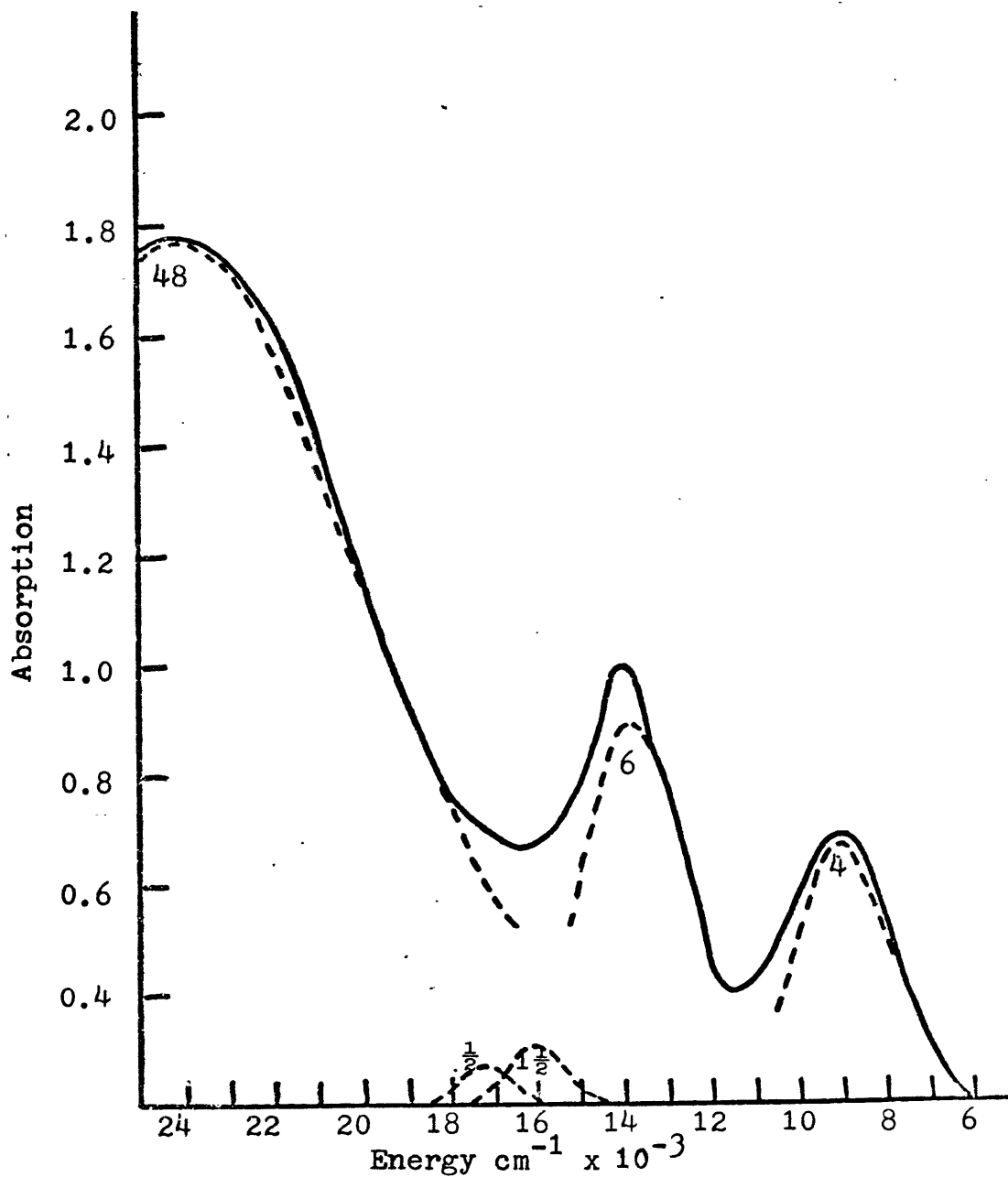


Figure 17. Polarized absorption spectrum of tourmaline #6. The figure shows the EIC spectrum fitted to component gaussian peaks, with percentage area of each peak.

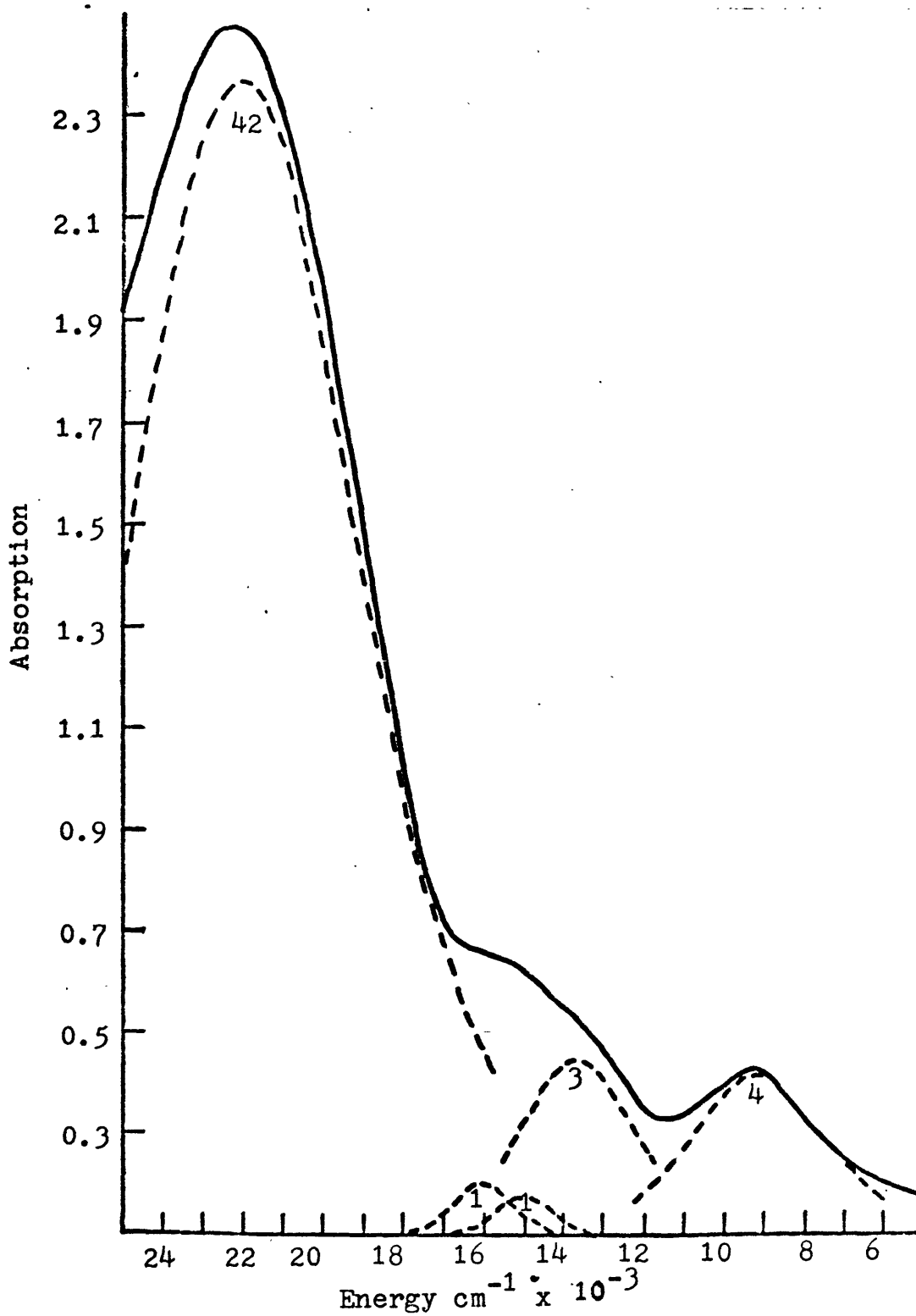


Figure 18. Polarized absorption spectrum of tourmaline #8. The figure shows the ELC spectrum fitted to component gaussian peaks, with percentage area of each peak.

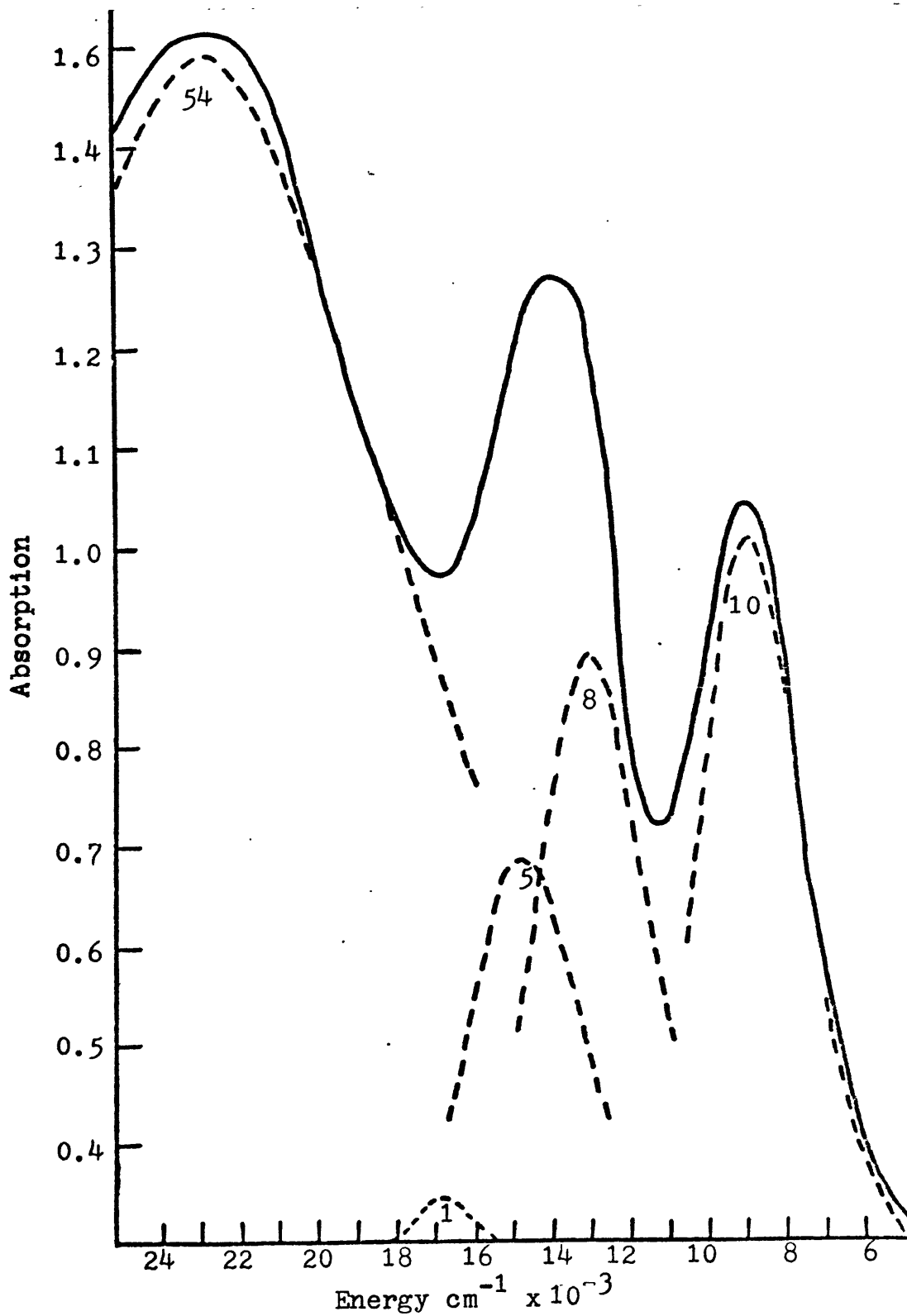


Figure 19. Polarized absorption spectrum of tourmaline #9. The figure shows the EIC spectrum fitted to component gaussian peaks, with percentage area of each peak.

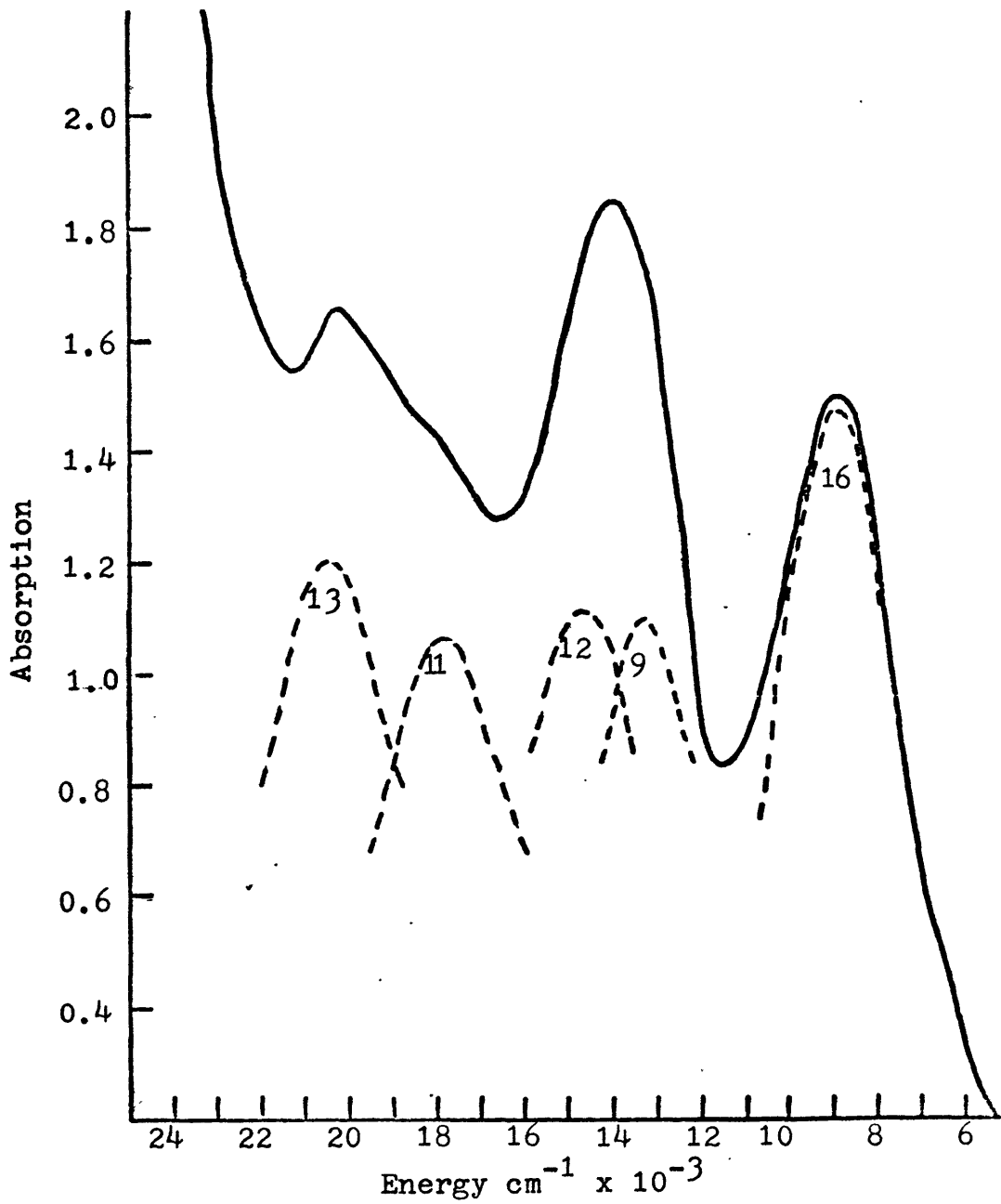


Figure 20. Polarized absorption spectrum of tourmaline #10. The figure shows the EIC spectrum fitted to component gaussian peaks, with percentage area of each peak.

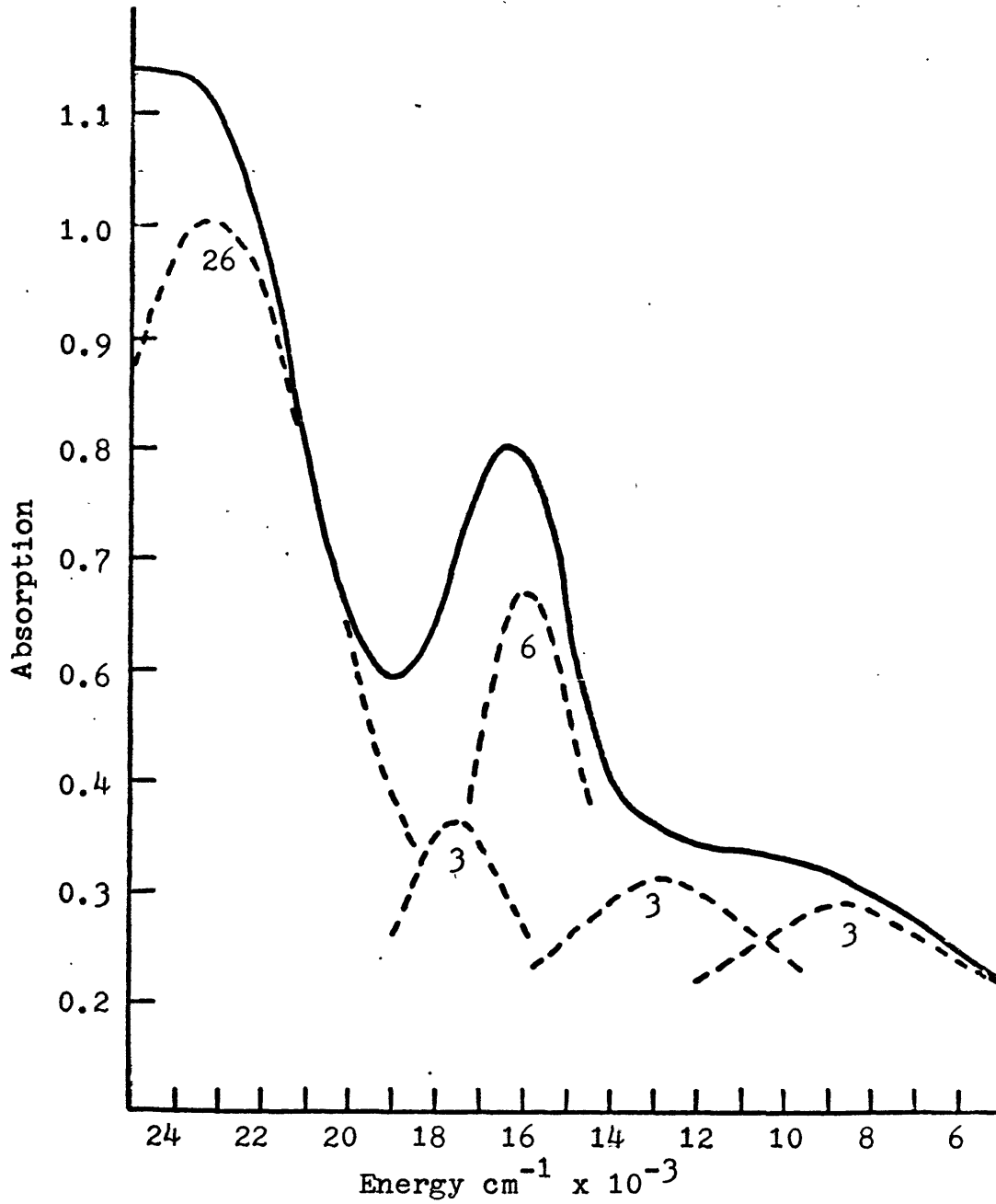


Figure 21. Polarized absorption spectrum of tourmaline #12. The figure shows the ELC spectrum fitted to component gaussian peaks, with percentage area of each peak.

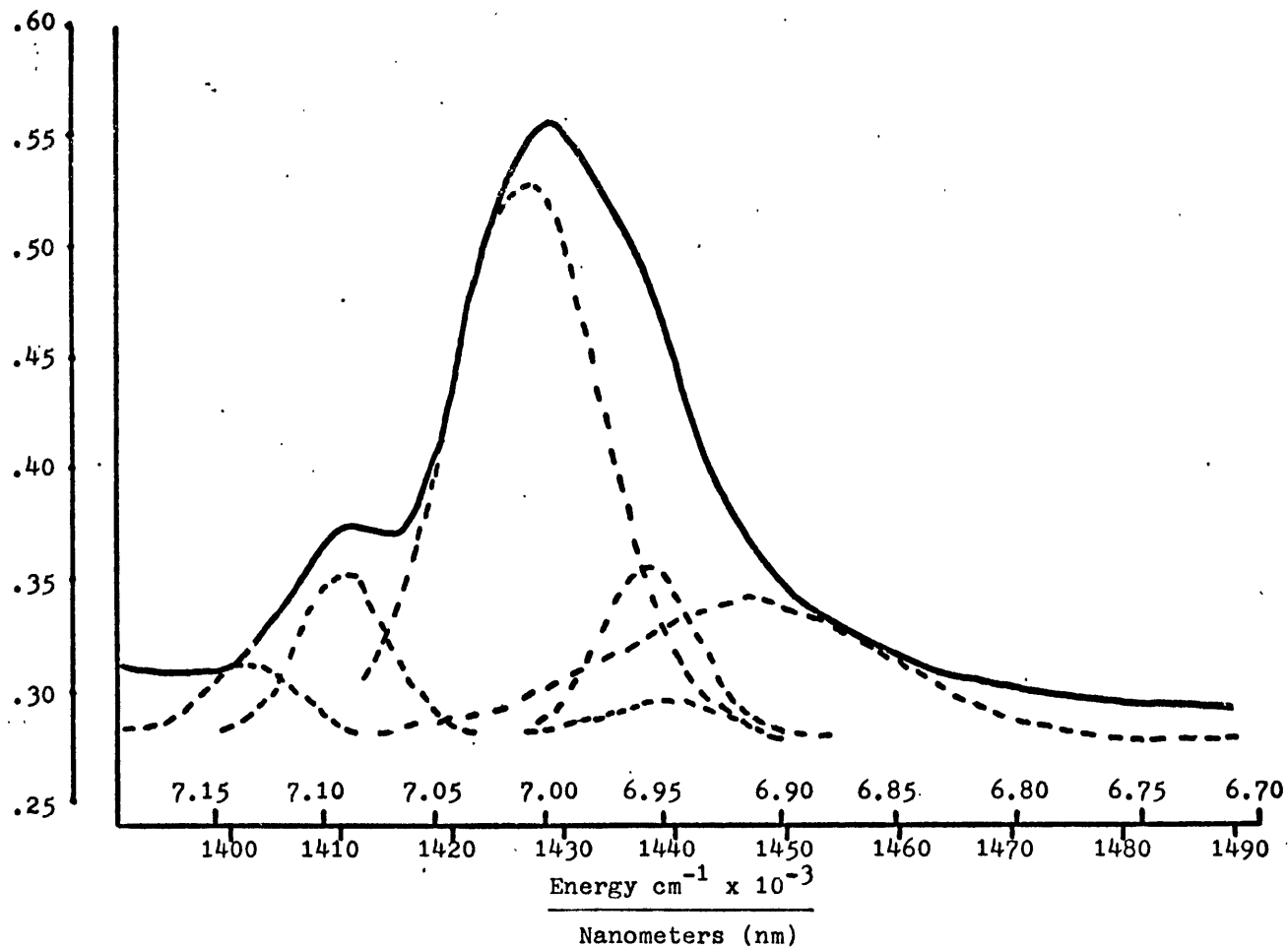


Figure 22. The first overtone, O-H bond, stretch spectrum of tourmaline #11. The absorption scale is normalized relative to the spectrum of #3 at 1490 nm., for easier comparison. (Actual peak intensities remain absolute.) The figure shows 6 component Gaussian peaks fitted to the spectral envelope.

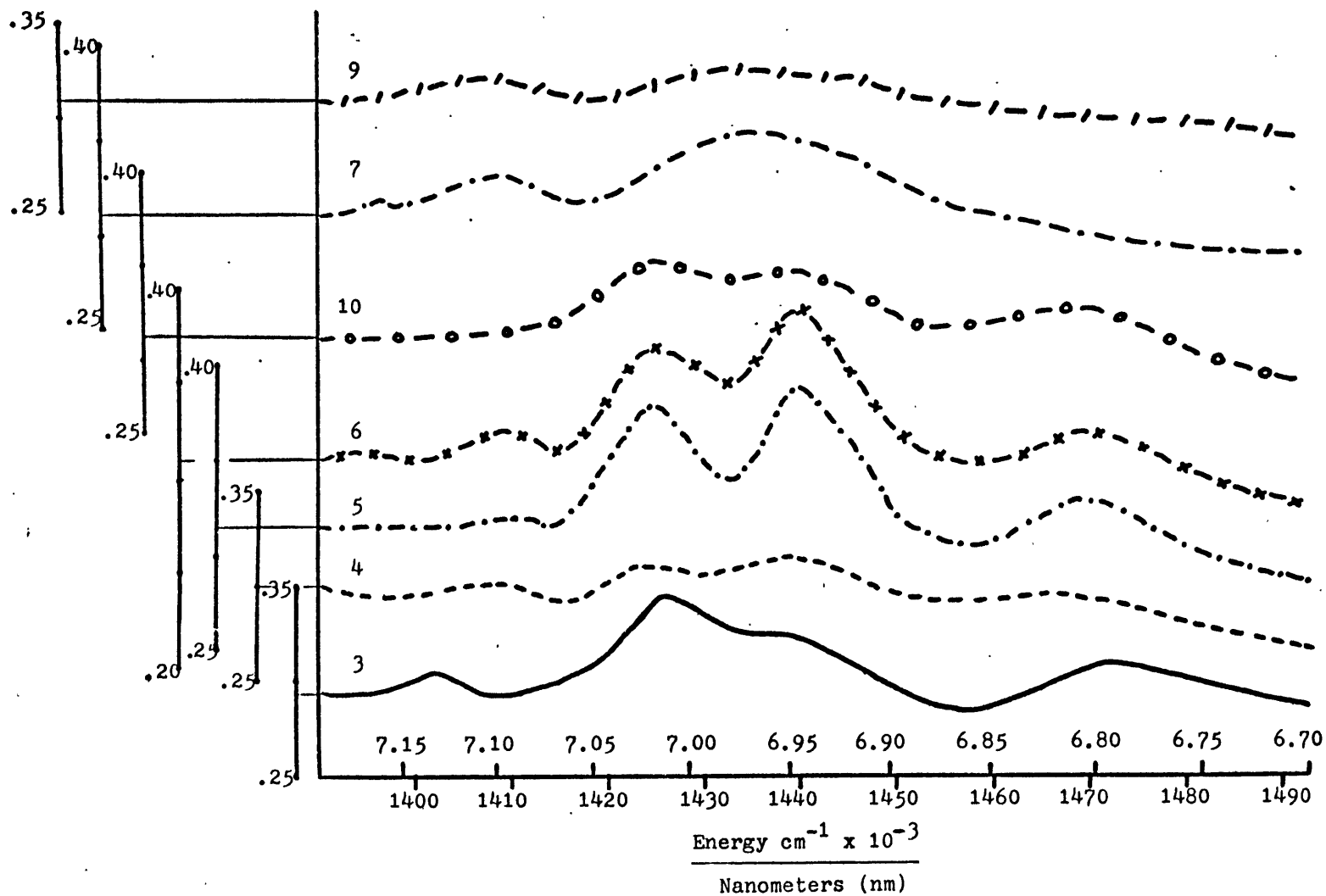


Figure 23. The first overtone, O-H bond, stretch spectra of tourmaline #3, 4, 5, 6, 7, 9, 10. All absorption scales are normalized relative to the spectrum of #3 at 1490 nm., for easier comparison. (Actual peak intensities remain absolute.) The figure reveals the peak trends at 1410, 1426, 1442, and 1470 nm.

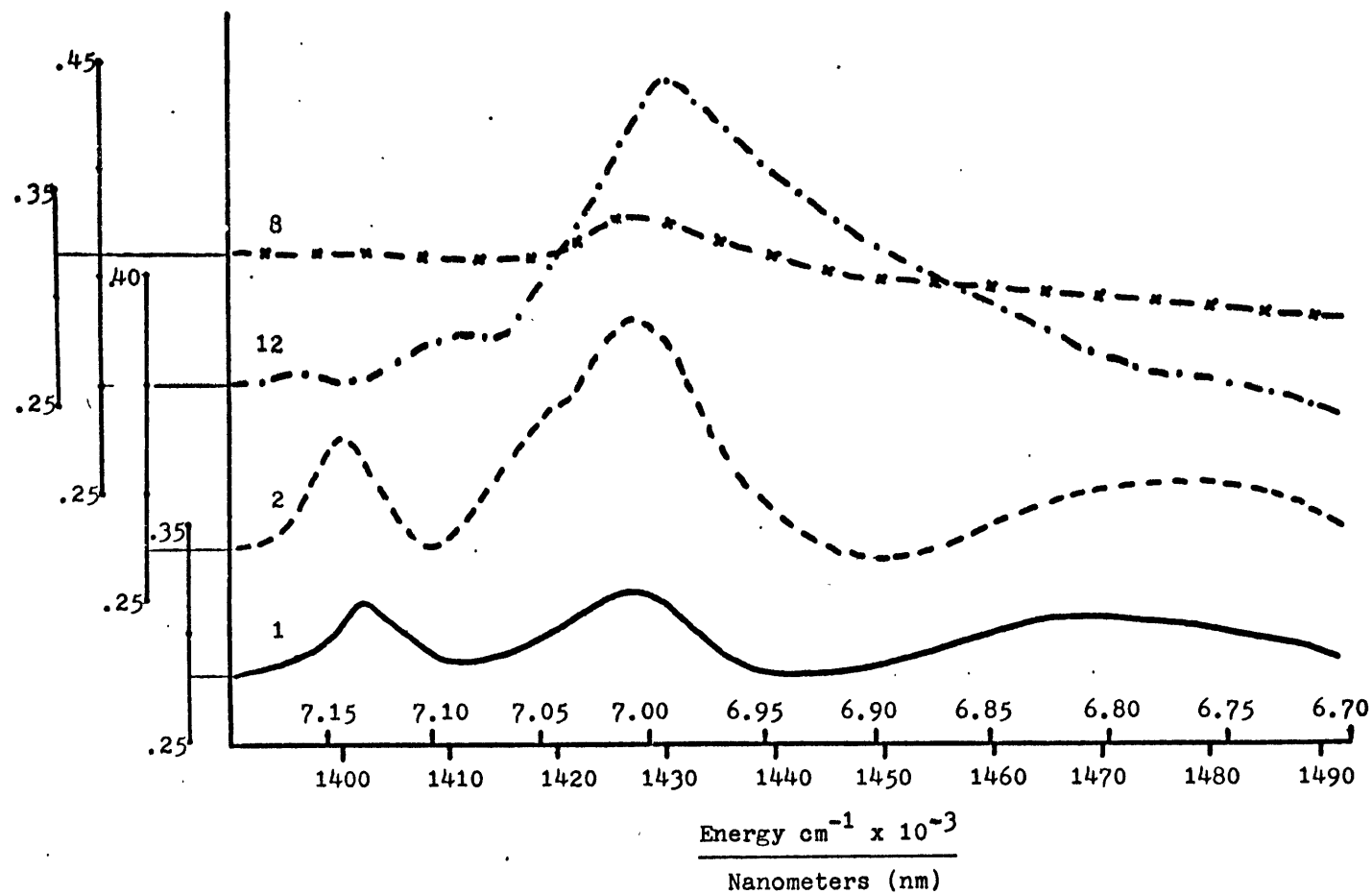


Figure 24. The first overtone, O-H bond, stretch spectra of tourmaline #1, 2, 8, 12. All absorption scales are normalized relative to the spectrum of #3 at 1490 nm., for easier comparison. (Actual peak intensities remain absolute.) The figure reveals the peak trends at 1400, 1430, and 1480 nm.

Chapter 4

RESULTS

4.1 Mössbauer Spectroscopy

The Mössbauer spectra of the eight iron bearing tourmalines are presented in Figures 5 through 12. Six of the spectra, those for specimens 3, 4, 5, 6, 8 and 9, consist of two large absorption peaks with asymmetric inner shoulders indicating the presence of a second, less intense doublet. Mössbauer spectra in earlier published literature (Marfunin, Mkrichyan, Nadzharyan, Nyussik and Platonov, 1970; Burns, 1972) have had assigned the more intense, outer doublet to the ferrous ion in the larger, 9(b) octahedral position, and the less intense, inner doublet to the ferrous ion in the smaller, 18(c) octahedral position. The remaining two spectra, for specimens 7 and 10, contain a much more pronounced shoulder on the inner side of the low velocity peaks, caused by ferric ions. Crystal structure determinations have shown that ferric ions occur in one or both octahedral sites in the tourmaline structure (Barton, 1969; Tippe et al., 1971).

Parameters obtained from the Mössbauer spectra are summarized in Tables 4 and 5. Chemical Shift (C.S.) and Quadrupole Splitting (Q.S.) are presented relative to the constraints indicated for each spectra in Figures 5 through 12. Halfwidth (H.W.), the ratio of the areas under each set of doublets, and

the x^2 values obtained from the computer fits are presented in relation to the number of constraints held, in each successive iteration of the computer fit.

The pale green (#3) and pale blue (#5) tourmaline fits diverged after lifting the "widths equal in pairs" constraints. This was due to the extreme overlap in peak positions, for which the computer could not compensate. The pale blue (htd) (#10) tourmaline diverged for similar reasons, and no fit was attempted with fewer than four constraints. The high iron, ferric bearing, black (#7) tourmaline proved to be too complex to resolve. A six peak fit was attempted, but the process diverged when any fit less than "fully constrained widths and intensities" was tried. The extremely high x^2 (1310) for #7 gave a strong indication of Fe^{3+} residency in both octahedral sites, which would necessarily lead to an eight peak fit.

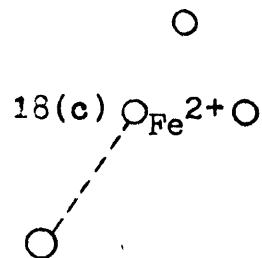
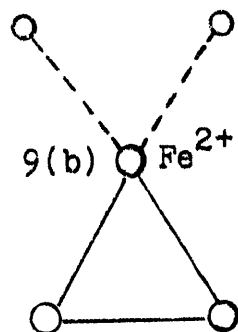
A comprehensive evaluation of the Mössbauer parameters in Tables 4 and 5 reveals certain trends which are highlighted herein. The Quadrupole Splitting (Q.S.) of both the outer and inner doublets of the totally ferrous tourmalines varies inversely to the amount of Mg^{2+} in the sample. Since the Quadrupole Splitting depends on the gradient of the electric field (which is actually a function of electron orbital distortion) produced by the other ions in the lattice (Wertheim, 1964), and since the electronegativity of Mg^{2+} is less than the electronegativity of Fe^{2+} , thereby causing less Fe^{2+} electronic dis-

tortion with increased Mg^{2+} over Fe^{2+} , the cause and effect relationship is substantiated. The tourmaline system, bearing Al^{3+} , does not follow, however, the well established rule in Mg^{2+} - Fe^{2+} , non- Al^{3+} bearing systems, that an increase in Fe^{2+} will cause a decrease in Q.S.

The Chemical Shift (C.S.) which measures the charge density of the atomic electrons at the nucleus (Wertheim, 1964) is valence dependent and is usually quite stable for an iron cation in a site in a crystal structure, irrespective of nearest neighbors. Mössbauer data compares favorably with this phenomenon with a maximum deviation for C.S. in the samples of ± 0.03 mm/sec.

Halfwidths at half-height of the doublets were one-quarter to one-half greater in the inner doublet than the outer doublet for Fe^{2+} specimens. An assessment of the site multiplicity combinations for each cation site reveals that, using only Mg^{2+} and Al^{3+} as substitute cations, there are nine different combinations in the 9(b) site with its nearest neighbors and six different combinations in the 18(c) site (see Figure 3). Table 6 shows the possible combinations with nearest neighbors. Each different combination represents a potential component, absorption peak at a finite, different energy. Since the Mössbauer spectrometer's resolution power is inadequate to differentiate between these closely overlapping peaks, the actual spectra show Lorentzian peaks with broadened shoulders, causing increased widths. The 9x (inner peak) to 6x (outer peak) ratio

Table 6. Combinations of Nearest Neighbor Cations with Fe^{2+} in the 9(b) and 18(c) tourmaline sites.



9(b)	9(b)	18(c)	18(c)
Mg	Mg	Al	Al
Mg	Mg	Al	Fe
Mg	Mg	Fe	Fe
Mg	Fe	Al	Al
Mg	Fe	Al	Fe
Mg	Fe	Fe	Fe
Fe	Fe	Al	Al
Fe	Fe	Al	Fe
Fe	Fe	Fe	Fe

9(b)	18(c)	18(c)
Mg	Al	Al
Mg	Al	Fe
Mg	Fe	Fe
Fe	Al	Al
Fe	Al	Fe
Fe	Fe	Fe

holds when additional cations are introduced into the structure. This is corroborated by experimental results shown in Tables 4 and 5.

Area ratios presented another trend which has its foundation in crystal field theory. As Fe^{2+} content increased with low Mg^{2+} (#3, 4, 5) the area ratio of outer doublet to inner doublet went down. This is indicative of more Fe^{2+} entering the smaller, 18(c) site. If Fe^{2+} content is held constant, and Mg^{2+} is increased while Al^{3+} is decreased, the ratio increases (e.g., #6). Fe^{2+} is allowed to enter the 9(b) site more readily, with the smaller Mg^{2+} ion moving into the 18(c) site. With low Fe^{2+} and high Mg^{2+} content, however, Fe^{2+} is more evenly distributed in both sites (#8, 2:1; #9, 1.3:1).

In the heated pale blue sample (#10), oxidation due to heating favors the smaller 18(c) site over the larger 9(b) site. Crystal field theory confirms this in that there is greater susceptibility to oxidize, and thereby reduce the size of, the Fe^{2+} in the more distorted Z octahedral site.

4.2 Optical/Near-infrared Spectroscopy

The optical/near-infrared spectra of nine tourmaline specimens are presented in Figures 13 through 21. The crystals were oriented with the c-axis perpendicular to the electric vector component of the polarized light source. Greater absorption was obtained in this orientation than in $E \parallel c$ due to the direction of bonding ($\perp c$) of the cations in the tourmaline

octahedral layer. Absorption is presented in absorption units with background absorption subtracted from the experimental data. Absolute absorption (the extinction coefficient) was not calculated due to the incomplete chemical analysis of specimens in the study. The linear data obtained on the horizontal scale was converted to energy units (cm^{-1}) in order for each envelope to be fitted with six component Gaussian curves. The component curves were fitted to give better peak resolution of each envelope.

The ultraviolet range ($30000\text{-}25000 \text{ cm}^{-1}$) and optical range ($25000\text{-}17000 \text{ cm}^{-1}$) peaks have been discussed at length previously, and have had electronic and crystal field assignments given them (Faye et al., 1968; Manning, 1968; Manning, 1969; Robbins and Strens, 1968; Wilkins et al., 1969).

An additional component peak, resolved at $\sim 15000 \text{ cm}^{-1}$ is analogous to the $\text{Fe}^{2+} \rightarrow \text{Fe}^{3+}$ intervalence transition peak in kyanite (16700 cm^{-1}) (Robbins et al., 1968; Faye and Nickel, 1969), in sapphire (11400 cm^{-1}) (Faye, 1971), in glaucophane ($15500\text{-}19000 \text{ cm}^{-1}$) (Bancroft and Burns, 1969) and riebeckite ($14300\text{-}17600 \text{ cm}^{-1}$) (Faye et al., 1970), and in vivianite (15200 cm^{-1}) (Faye et al., 1968).

The spectra are separated into two categories: the identifiable iron content specimens (#3, 4, 5, 6, 8, 9, 10) and the iron free specimens (#1 and 12). This distinction was made to facilitate subsequent comparison with Mössbauer spectra.

All the iron bearing tourmalines contained two distinct peaks at 14000 and 9000 cm^{-1} . The 9000 cm^{-1} peak is the result of Fe^{2+} in the larger 9(b), octahedral site in tourmaline (Faye et al., 1968; Robbins et al., 1968; Manning, 1969; Wilkins et al.; 1969).

The 14000 cm^{-1} peak exhibited definite trends in its relative area relationship with the 9000 cm^{-1} peak, which were influenced by chemical composition and by site occupancy in the 9(b) and 18(c) octahedral sites. With a high content of Al^{3+} (Al in 9(b) and 18(c) sites), an increase in Fe^{2+} caused a relative increase in both 14000 and 9000 cm^{-1} peak areas (#3, 4 and 5). The intervalence transition peak (15000 cm^{-1}) area followed the 14000 cm^{-1} peak area proportionately (see Figures 14, 15 and 16).

A slight decrease in Fe^{2+} , coupled with a large increase in Mg^{2+} (#6), caused an abrupt drop in the intervalence transition peak area, with a corresponding turnabout in relative areas of the 14000 and 9000 cm^{-1} peaks (see Figure 17).

The two low iron specimens (#8 and 9) produced peak areas relatively equal to each other, with the intervalence transition peak area holding to a steady ratio with the 14000 cm^{-1} peak area (see Figures 18 and 19).

The heating of #5, producing specimen #10, shows an increase in the $\text{Fe}^{2+} \rightarrow \text{Fe}^{3+}$ intervalence transition peak area at the expense of the 14000 cm^{-1} peak area (see Figure 20).

The specimens containing little or no iron (#1 and 12) do not show the 14000 and 9000 cm^{-1} peaks, but rather peaks which are finitely shifted from these positions.

4.3 First-overtone, O-H Bond, Stretch Spectra

The first-overtone, O-H bond, stretch spectra for all the tourmaline specimens examined in this study are presented in Figures 22 through 24. The crystals were oriented with the c-axis parallel to the electric vector component of the polarized light source. There was no evidence in the $E \parallel c$ orientation of the stretch bands, which strengthens the hypothesis that both O-H site bonds lie parallel to the c-axis. The samples were categorized according to a predominance of iron (Figure 23) or magnesium (Figure 24) per formula unit. Specimen #11 was extracted from the magnesium group, and was fitted with six component Gaussian curves. This tourmaline approximated the ideal dravite structure, and was used as a standard of comparison between the two groups since it had virtually no iron in its composition. The absorption scales were normalized relative to the pale green (#3) tourmaline for easier comparison. The intensities and energy positions of the peaks were not altered.

Certain peak trends were observed in each figure. The predominantly iron specimens displayed peaks at 1410, 1426, 1442, and 1470 nm. Other less intense inflections were noted, but do not predominate in all specimens. The high magnesium

bearing samples show peak trends at 1400, 1430, and 1480 nm. Sample #11 presented a dominant peak at 1430 nm with a shoulder inflection at 1410 nm.

Tourmalines contain two O-H sites. Cation co-ordination in each site is illustrated in Figure 4. Due to the fact that each cation site bonded to an O-H site may contain a multiplicity of cations, there is a maximum number of combinations, and hence environments, of cations to which the O-H anion can bond. Alkali amphiboles have an analogous O-H bonding situation to the tourmaline O_3 (OH_{II}) site with one Y and two Z nearest neighbor cations. Bancroft and Burns (1969), in a study of these amphiboles, proposed that with three cation sites, M(1), M(3), M(1), and with four cations (Mg^{2+} , Fe^{2+} , Fe^{3+} , Al^{3+}) involved in site multiplicity arrangements, twenty different combinations (sixty-four permutations) could be either position identified or statistically assumed in the alkali amphibole O-H bond, stretch spectra. In applying this hypothesis to the present study, additional cations (Li^{1+} , Mn^{2+} , Mn^{3+} , Ti^{4+}) must be included in varying amounts in the 9(b) and 18(c) sites in the tourmaline structure. Coupling this situation with the $O_1(OH_I)$ site in tourmaline, with three Y and one X nearest neighbor cations, basic statistical analysis reveals that the possibilities of site multiplicity combinations grows rapidly with each cation added to the system. Since each combination generates its own distinct energy absorption peak within the

first-overtone, O-H bond, absorption bands, there is necessarily considerable overlap in absorption peaks.

Crystal field theory can be called upon to estimate relative positions of cation absorption peaks on the energy scale (Burns, private communications, 1973). Table 7 shows the trend of cation-oxygen bonding to oxygen-hydrogen bonding. The oxygen-hydrogen bond intensity determines the relative position of the absorption peak on the energy (cm^{-1}) scale. The weaker the cation-oxygen bond, the stronger the oxygen-hydrogen bond, and the further left (higher energy) the position of the absorption peak.

In illustration of simple cation multiplicity, a system of Mg^{2+} and Al^{3+} only is presented in Table 8 for the two O-H sites. Utilizing this theory of cation peak positioning and the six component Gaussian peak fit in Figure 22, one can at least show trends in peak position vs. chemical composition (from Table 3). Lithium, being the weakest bonding cation, would develop a peak at the highest energy bond for O-H (furthest left on energy scale). Such a peak trend appears at ~ 1400 nm in specimens #1, 2 and 3, which presumably have a high Li^{1+} content. Mg^{2+} content influences the broad peak at ~ 1430 nm. Another trend of inflections at ~ 1442 nm are influenced by Fe^{2+} content; and a fourth broad peak trend at ~ 1480 nm seems to be affected by Al^{3+} content. All other cations are present in such small amounts that it is impossible to resolve any inflections

Table 7. Comparison of the Cation-Oxygen Bond to the Oxygen-Hydrogen Bond in the Hydroxyl sites in the tourmaline structure.


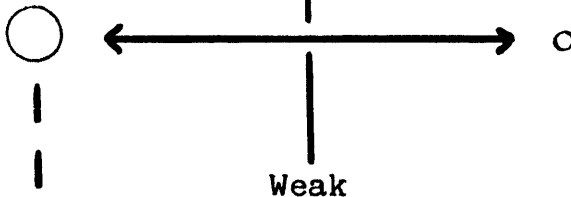
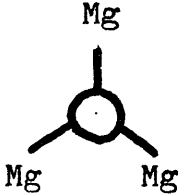
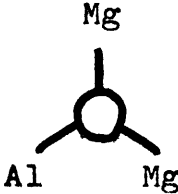
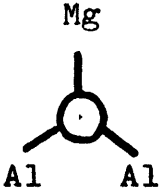
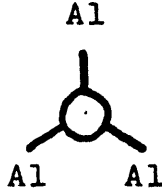
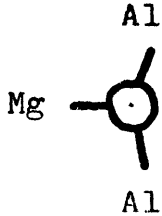
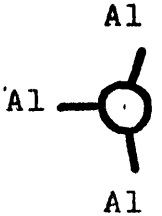
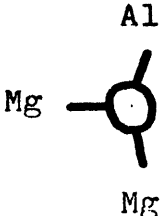
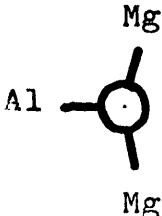
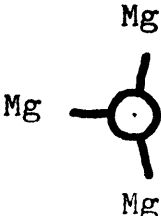
Cations	Cation-Oxygen Bond	Oxygen-Hydrogen Bond
Li ¹⁺	Weak  Strong	
Mg ²⁺		
Mn ²⁺		
Fe ²⁺		
Al ³⁺		
Fe ³⁺		
Mn ³⁺	Increase in energy to vibrate O - H bond	

Table 8. Cation site multiplicity for a $Mg^{2+} - Al^{3+}$ system in the O - H sites in the tourmaline structure.

<u>Type</u>	Probability				
	Most	←	→	Least	
$O_1(OH_I)$					
$O_3(OH_{II})$					

made by them. The six peak fit represented only a first step in the establishment of complete resolution and identification of O-H bond absorption peaks.

Assignment of peak intensities and thereby site occupation was not attempted since absorption was obtained in absorption units, and could not be converted to absolute absorption (extinction co-efficients) without a complete chemical analysis.

Chapter 5

DISCUSSION OF RESULTS

5.1 Mössbauer Spectroscopy

The Mössbauer data have substantiated the findings of earlier studies that Fe^{2+} and Fe^{3+} cations are contained in both octahedral sites in the tourmaline structure (Marfunin et al., 1970; Burns, 1972). All the iron-bearing specimens measured in this study exhibited inner shoulders in their Mössbauer spectra. The spectra were resolved into at least two ferrous doublets, when fitted with component Lorentzian curves.

Site populations of the ferrous cations were also quantitatively estimated by the use of relative areas under each doublet. It was apparent that as the iron content of a tourmaline increased, greater proportions of the 18(c) octahedral site were populated by ferrous iron. However, the relative proportion of Fe^{2+} ions in the 9(b) sites increased with rising magnesium concentration in tourmalines of comparable iron content. This suggested a process of Fe^{2+} being forced into the 9(b) site as a result of the smaller magnesium cation readily occupying the smaller 18(c) position.

The Mössbauer spectroscopy also revealed that the oxidation process of ferrous iron in tourmaline is favored in the 18(c) site. This was evidenced by an increase in the outer ferrous iron doublet relative to the inner doublet with simultaneous

appearance of a ferric iron doublet.

5.2 Optical/Near-infrared Spectroscopy

Optical/near-infrared spectroscopy substantiated the existence of an intervalence transition band in tourmalines. This band at $\sim 15000 \text{ cm}^{-1}$ is analogous to the $\text{Fe}^{2+} \rightarrow \text{Fe}^{3+}$ intervalence transition bands found in other silicate minerals (Burns, 1970). The component Gaussian curves fitted to a spectral envelope also substantiated earlier studies (Faye et al., 1968; Robbins et al., 1968; Manning, 1969; Wilkins et al., 1969) in which the 9000 cm^{-1} band was assigned to Fe^{2+} ions in the tourmaline 9(b) sites. The curve-fitting also resolved an additional peak at 14000 cm^{-1} , attributed to Fe^{2+} ions in the tourmaline 18(c) sites.

5.3 Comparison of Mössbauer - Optical/Near-infrared Results

Correlations of Mössbauer and optical/near-infrared data confirmed the assignment of the 14000 cm^{-1} peak to ferrous iron residency in the 18(c) octahedral site in tourmalines.

An increase in iron content in the elbaite-schorl series caused an increase in both the 14000 and 9000 cm^{-1} peak areas in the optical/near-infrared spectra. A large increase in magnesium caused a decrease in the 15000 cm^{-1} intervalence transition peak. This trend is explicable in terms of more ferrous iron being forced into the larger 9(b) site and being involved in fewer intervalence transitions, compared to the

situation when there is a large occupancy of the 18(c) sites.

This increase in 9(b) site occupancy in magnesium tourmalines correlates with an increase in the outer/inner ferrous doublet area ratio in the Mössbauer spectra.

The oxidation process of iron is demonstrated by peak intensity stealing of the 14000 cm^{-1} peak in the optical/near-infrared spectra and by peak intensity stealing of the inner, 18(c) site, ferrous doublet in the Mössbauer spectra.

In specimens of the elbaite-schorl series, however, a DECREASE in relative $14000/9000\text{ cm}^{-1}$ peak areas did not materialize. Similarly, and INCREASE in the peak area ratio was not observed in elbaite-schorl #6.

Except for specimen 6, the correlations between the two spectroscopic methods are statistically satisfactory, given the limitations of the technique in fitting Gaussian curves to electronic spectra. The two assumptions initially made may have influenced the interpretation of the optical/near-infrared spectral data. First, the absorption baseline was assumed to be linear throughout the spectral range. Background absorption was subtracted from the spectral envelope to arrive at the actual experimental data. Second, significant absorption in the ultraviolet range was compensated for by a very large Gaussian peak, centered in the near-ultraviolet and ultraviolet range. Other authors (Faye and Nickel, 1970) have superimposed fitted Gaussian peaks on a baseline which increased almost

exponentially in absorbance from $\sim 10000 \rightarrow 25000 \text{ cm}^{-1}$.

5.4 First-overtone, O-H Bond, Stretch Spectra

The investigation of the first-overtone, O-H bond, stretch spectra gave qualitative trends only. The spectra proved to be too complex to resolve in any quantitative manner. The number of peaks, coupled with their close positioning relative to each other, made it impossible to make any definite peak assignments. Certain peak trends, however, could be noted. Applying a Crystal Field Theory axiom, namely, that ordering of cations on a bond-energy scale was possible due to the greater polarizing power of M^{3+} cations over M^{2+} cations, allowed the assignment of certain high population cations to specific peak trends.

The inflection trend at $\sim 1403 \text{ nm}$ can be assigned to Li^{1+} . Specimens exhibiting this peak were positioned by their cell parameters on the elbaite end of the elbaite-schorl join and are assumed to have a high concentration of lithium. The peak at $\sim 1426 \text{ nm}$, appears to be related to magnesium. A third trend, namely ferrous iron at $\sim 1442 \text{ nm}$ is accentuated in all iron-bearing tourmalines. A ferric iron position could not be identified. Peak overlap and low content are plausible explanations for this absence. A final trend was noted at $\sim 1470 \text{ nm}$. This was attributed to aluminum since the intensity and width of this peak closely correlated with the Al^{3+} content in the specimens.

In summary, the use of Mössbauer spectroscopy confirmed the presence of ferrous iron in both octahedral sites in tourmaline. Optical/near-infrared spectroscopy, though not as quantitative as Mössbauer spectroscopy, was used in connection with Mössbauer data to establish the designation of the absorption peak at 14000 cm^{-1} as the result of ferrous iron residency in the 18(c) octahedral site in tourmaline.

REFERENCES

- Bancroft, G.M., and R.G. Burns (1967), "Applications of The Mössbauer Effect to Mineralogy." Fifth Int. Mineral. Assoc. Meeting. Symposium I. Ontario, Canada.
- _____, and _____ (1969), "Mössbauer and Absorption Spectral Study of Alkali Amphiboles." Mineral. Soc. Amer., Spec. Pap. 2, 137-148.
- _____, _____, and R.A. Howie (1967), "Determination of Cation Distribution in Orthopyroxene by the Mössbauer Effect." Nature, 213, 1221-1223.
- _____, _____, and A.G. Maddock (1967), "Determination of Cation Distribution in the Cummingtonite-Grunerite Series by Mössbauer Spectra." Amer. Mineral. 52, 1009-1026.
- _____, _____, _____, and R.G.J. Strens (1966), "Cation Distribution in Anthophyllite from Mössbauer and Infrared Spectroscopy." Nature, 212, 913-195.
- _____, A.G. Maddock, and R.G. Burns (1967), "Applications of the Mössbauer Effect to Silicate Mineralogy. I. Iron Silicates of Known Crystal Structure." Geochim. Cosmochim. Acta. 31, 2219-2246.
- Barton, R. Jr. (1969), "Refinement of the Crystal Structure of Buergerite and the Absolute Orientation of Tourmalines." Acta Cryst. B25, 1524-1533.
- Buerger, M.J., C.W. Burnham, and D.R. Peacor (1962), "Assessment of the Several Structures Proposed for Tourmalines." Acta Cryst. 15, 583-590.
- Burns, R.G. (1966), "Apparatus for Measuring Polarized Absorption Spectra of Small Crystals." J. Sci. Instr. 43, 58-60.
- _____. (1968), "Enrichments of Transition-metal Ions in Silicate Crystal Structures." In: L.H. Ahrens (ed.) Origin and Distribution of the Elements. Pergamon, New York. p. 1151-1164.
- _____. (1970), "Mineralogical Applications of Crystal Field Theory." Cambridge University Press, England.

- _____. (1972), "Mixed Valencies and Site Occupancies of Iron in Silicate Minerals from Mössbauer Spectroscopy." Can. J. of Spectroscopy 17, No. 2, 51-59.
- _____, and C.J. Greaves (1971), "Correlations of Infrared and Mössbauer Site Population Measurements of Actinolites." Amer. Mineral. 56, 2010-2033.
- _____, and R.G.J. Strens (1966), "Infrared Study of the Hydroxyl Bands in Clinoamphiboles." Science 153, 890-892.
- Donnay, G., and R. Barton Jr. (1972), "Refinement of the Crystal Structure of Elbaite and the Mechanism of Solid Solution." TMPM Tschermaks Mineral. Petr. Mitt. 18, 273-286.
- Duncan, J.F., and R.M. Golding (1965), "Mössbauer Studies of Chemical Bonding." Quart. Rev. 19, 36-56.
- Faye, G.H. (1968), "The Optical Absorption Spectra of Iron in Six-coordinate Sites in Chlorite, Biotite, Phlogopite, and Vivianite. Some Aspects of Pleochroism in the Sheet Silicates." Can. Mineral. 9, 403-425.
- _____. (1971), "On the Optical Spectra of Di- and Trivalent Iron in Corundum: A Discussion." Amer. Mineral. 56, 344-350.
- _____, P.G. Manning, and E.H. Nickel (1968), "The Polarized Optical Absorption Spectra of Tourmaline, Cordierite, Chloritoid and Vivianite: Ferrous-Ferric Electronic Interaction as a Source of Pleochroism." Amer. Mineral. 53, 1174-1201.
- _____, E.H. Nickel (1969), "On the Origin of Colour and Pleochroism of Kyanite." Can. Mineral. 10, 35-46.
- _____, _____ (1970), "The Effect of Charge-transfer Processes on the Colour and Pleochroism of Amphiboles." Can. Mineral. 10, 616-635.
- Fluck, E. (1964), "The Mössbauer Effect and Its Applications in Chemistry." In: H.J. Emeleus and A.G. Sharpe (ed.) Advances in Inorganic and Radiochemistry. Academic Press, New York and London. 433-489.
- Frauenfelder, H. (1962), "The Mössbauer Effect." W.A. Benjamin, Inc.

- Fron del, C., A. Biedl, and J. Ito (1966), "New Type of Ferric Iron Tourmaline." Amer. Mineral. 51, 1501-1505.
- Ito, T., and R. Sadanaga (1951), Acta Cryst. 4, 385.
- Manning, P.G. (1968), "An Optical Absorption Study of the Origin of Colour and Pleochroism in Pink and Brown Tourmalines." Can. Mineral. 9, 678-690.
- ____ (1969), "Optical Absorption Spectra of Chromium-bearing Tourmaline, Black Tourmaline, and Buergerite." Can. Mineral. 10, part I, 57-70.
- Marfunin, A.S., A.R. Mkrichyan, G.N. Nadzharyan, Y.M. Nyvssik, and A.N. Platonov (1970), Izv. Akad. Nauk. S.S.S.R., Ser. Geol., 2, 146.
- Novozhilov, A.I., I.E. Voskresenkaya, and M.I. Samoilovich (1969), "Electron Paramagnetic Resonance Study of Tourmalines." Soviet Physics - Crystallography 14, No. 3, 413-418.
- Plyusnina, I.I., B.G. Granadchikova, and I.E. Voskresenkaya (1969), "An Infrared Spectroscopic Study of Tourmalines." Soviet Physics - Crystallography 14, No. 3, 370-375.
- Robbins, D.W., and R.G.J. Strens (1968), "Polarization-dependence and Oscillator Strengths of Metal-metal Charge-transfer Bands in Iron (II, III) Silicate Minerals." Chem. Comm., 508-510.
- Shannon, R.D., and C.T. Prewitt (1969), "Effective Ionic Radii in Oxides and Fluorides." Acta Cryst. B25, 925-946.
- Stone, A.J., H.J. Aagard, and J. Fenger (1971), Danish Atomic Energy Comm., RISO-M-1348 -- [Nucl. Sci. Abstr., 25, 30688 (1971)].
- Tippe, A., and W.C. Hamilton (1971), "A Neutron Diffraction Study of the Ferric Tourmaline, Buergerite." Amer. Mineral. 56, 101-113.
- Townsend, M.G. (1970), "On the Dichroism of Tourmaline." J. Phys. Chem. Solids 31, 2481-2488.
- Tsang, T., A.N. Thorpe, G. Donnay, and F.E. Senftle (1971), "Magnetic Susceptibility and Triangular Exchange Coupling in the Tourmaline Mineral Group." J. Phys. Chem. Solids 32, 1441-1448.

_____, and S. Ghose (1973), "Nuclear Magnetic Resonance of ^1H , ^7Li , ^{11}B , ^{23}Na , and ^{27}Al in Tourmaline (Elbaite)." Amer. Mineral. 58, 224-229.

Vaughan, D.J. and R.G. Burns (1972), "Mössbauer Spectroscopy and Bonding in Sulphide Minerals Containing Four-co-ordinated Iron." 24th Int. Geol. Congr. Sec. 14, 158-167.

Wilkins, R.W.T., E.F. Farrell, and C.S. Naiman (1969), "The Crystal Field Spectra and Dichroism of Tourmaline." J. Phys. Chem. Solids 30, 43-56.

Wertheim, G.K. (1964), Mössbauer Effect: Principles and Applications. Academic Press, New York and London.